JEM Journal of Experimental Medicine

ARTICLE

E3 ligase MKRN3 is a tumor suppressor regulating PABPC1 ubiquitination in non–small cell lung cancer

Ke Li[1*], Xufen Zheng[1*], Hua Tang[2*], Yuan-Sheng Zang[3*], Chunling Zeng[1], Xiaoxiao Liu[1], Yanying Shen[5], Yuzhi Pang[1], Simin Wang[1], Feifei Xie[1], Xiaojing Lu[1], Yuxiang Luo[1], Zhang Li[1], Wenbo Bi[1], Xiaona Jia[1], Tao Huang[6], Rongqiang Wei[2], Kenan Huang[2], Zihao Chen[2], Qingchen Zhu[8], Yi He[9], Miaoying Zhang[12], Zhizhan Gu[10,11], Yichuan Xiao[8], Xiaoyang Zhang[7], Jonathan A. Fletcher[4], and Yuexiang Wang[1]

Central precocious puberty (CPP), largely caused by germline mutations in the *MKRN3* gene, has been epidemiologically linked to cancers. *MKRN3* is frequently mutated in non–small cell lung cancers (NSCLCs) with five cohorts. Genomic *MKRN3* aberrations are significantly enriched in NSCLC samples harboring oncogenic *KRAS* mutations. Low MKRN3 expression levels correlate with poor patient survival. Reconstitution of MKRN3 in MKRN3-inactivated NSCLC cells directly abrogates in vitro and in vivo tumor growth and proliferation. *MKRN3* knockout mice are susceptible to urethane-induced lung cancer, and lung cell–specific knockout of endogenous *MKRN3* accelerates NSCLC tumorigenesis in vivo. A mass spectrometry–based proteomics screen identified PABPC1 as a major substrate for MKRN3. The tumor suppressor function of MKRN3 is dependent on its E3 ligase activity, and *MKRN3* missense mutations identified in patients substantially compromise MKRN3-mediated PABPC1 ubiquitination. Furthermore, MKRN3 modulates cell proliferation through PABPC1 nonproteolytic ubiquitination and subsequently, PABPC1-mediated global protein synthesis. Our integrated approaches demonstrate that the CPP-associated gene *MKRN3* is a tumor suppressor.

Introduction

Lung cancer is the leading cause of cancer-related mortality worldwide, with 2,093,876 new cases and 1,761,007 deaths globally in 2018 (Hellmann et al., 2019; Siegel et al., 2020; Teixeira et al., 2019). Approximately 85% of all lung cancer cases are non–small cell lung cancers (NSCLCs; Campbell et al., 2016; Peifer et al., 2012). NSCLCs mostly include lung adenocarcinoma and lung squamous cell carcinoma (Campbell et al., 2016). Although tyrosine kinase inhibitors and immunotherapy have contributed to significant survival benefits in some patients, the overall survival rates for NSCLCs remain low. In particular, patients with NSCLC that is driven by *KRAS* mutations are often unresponsive to tyrosine kinase inhibitors and have a poor prognosis (Mainardi et al., 2018). For patients with NSCLC who harbor mutations in the epidermal growth factor receptor (*EGFR*) or in anaplastic lymphoma kinase (*ALK*) fusions, targeted therapies are now the first-line standard of care (Govindan et al., 2012; Imielinski et al., 2012; Pao and Chmielecki, 2010; Shaw and Engelman, 2013); in contrast, targeted therapy against mutant KRAS-driven tumors (in up to 30% of NSCLCs) has proved challenging (Hellmann et al., 2019; Mainardi et al., 2018). Indeed, although allele-specific inhibitors for the $KRAS^{G12C}$ mutant have entered phase I clinical trials, a general strategy that targets all KRAS mutants remains elusive (Hong et al., 2020). There is therefore an urgent need to identify new driver genes and develop therapeutic strategies to benefit a broader patient population, especially those with *KRAS* mutations.

[1]Chinese Academy of Sciences Key Laboratory of Tissue Microenvironment and Tumor, Shanghai Institute of Nutrition and Health–Changzheng Hospital Joint Center for Translational Medicine, Institutes for Translational Medicine, Shanghai Institute of Nutrition and Health, University of Chinese Academy of Sciences, Chinese Academy of Sciences, Shanghai, China; [2]Department of Thoracic Surgery, Changzheng Hospital, Shanghai, China; [3]Department of Medical Oncology, Changzheng Hospital, Shanghai, China; [4]Department of Pathology, Brigham and Women's Hospital and Harvard Medical School, Boston, MA; [5]Department of Pathology, Ren Ji Hospital, School of Medicine, Shanghai Jiao Tong University, Shanghai, China; [6]Bioinformatics Core, Shanghai Institute of Nutrition and Health, Shanghai Institutes for Biological Sciences, Chinese Academy of Sciences, Shanghai, China; [7]Department of Oncological Sciences, Huntsman Cancer Institute, University of Utah, Salt Lake City, UT; [8]Chinese Academy of Sciences Key Laboratory of Tissue Microenvironment and Tumor, Shanghai Institute of Nutrition and Health, Shanghai Institutes for Biological Sciences, Chinese Academy of Sciences, University of Chinese Academy of Sciences, Shanghai, China; [9]Department of Urology, No. 1 Hospital of Jiaxing, Jiaxing, China; [10]Department of Cancer Immunology and Immune Modulation, Boehringer Ingelheim Pharmaceuticals, Inc., Ridgefield, CT; [11]Department of Anatomy and Structural Biology and Gruss Lipper Biophotonics Center, Albert Einstein College of Medicine, Bronx, NY; [12]Department of Pediatric Endocrinology and Inherited Metabolic Diseases, Children's Hospital of Fudan University, Shanghai, China.

*K. Li, X. Zheng, H. Tang, and Y.-S. Zang contributed equally to this paper; Correspondence to Yuexiang Wang: yxwang76@sibs.ac.cn.

Central precocious puberty (CPP) is largely caused by germline mutations in the Makorin ring finger protein 3 (*MKRN3*: reference transcript, NM_005664; reference protein, NP_0056550) gene (Abreu et al., 2013). The molecular function of MKRN3 in CPP is a subject of considerable investigation (Abreu et al., 2013; Abreu et al., 2020; Shin, 2016). Interestingly, CPP has been epidemiologically linked to various diseases in adulthood, including cancers (Day et al., 2017; Holmes, 2017). Cohorts of individuals with CPP show an increased risk (~10–25%) of malignancies such as lung cancers (Ben Khedher et al., 2017; Calcaterra et al., 2013; Kreuzer et al., 2003). There is also compelling evidence that sex steroid hormones and reproductive factors play a role in the genesis of lung cancer (Ben Khedher et al., 2017; Kreuzer et al., 2003), yet the mechanisms are unclear.

Cancer cells require high global protein translation rates to maintain their fast proliferation behavior. Protein synthesis is a major metabolic event that controls cancer cellular growth and proliferation, but its precise regulatory mechanisms in cancer are not well understood (Bretones et al., 2018; Ebright et al., 2020; Lindqvist et al., 2018; Nguyen et al., 2018; Pelletier et al., 2018).

To investigate whether MKRN3 functions in human cancers, we analyzed the public data from cancer genomics studies and found recurrent inactivating genomic *MKRN3* aberrations in NSCLCs. We further present genetic, functional, genetically engineered mouse model and mechanistic data that identify the *MKRN3* gene at 15q11 as a bona fide tumor suppressor in NSCLCs and uncover a potential therapeutic target in *KRAS*-mutant lung cancer.

Results

MKRN3 is frequently altered in NSCLCs, and reduced expression correlates with poor patient survival

To investigate whether CPP-associated *MKRN3* gene is mutated in human cancers, we queried The Cancer Genome Atlas (TCGA) Pan-Cancer genomic datasets. Frequent *MKRN3* alterations were detected in the TCGA Pan-Cancer genomic dataset containing 566 samples of lung adenocarcinoma, the most common type of NSCLC. *MKRN3* alterations were identified in 5.0% (28 of 566) of lung adenocarcinoma samples (Fig. 1 A). We further detected a 2–6% *MKRN3* alteration rate in four additional NSCLC cohorts consisting of lung adenocarcinomas and lung squamous cell carcinomas similarly examined by whole-genome/whole-exome sequencing (Fig. 1 A). Genomic *MKRN3* aberrations are significantly enriched in human NSCLC samples harboring oncogenic *KRAS* mutations (Fig. S1 A; $P < 0.05$, discrete independence statistic controlling for observations with varying event rate [DISCOVER] test; Table 1). Collectively, these data established an *MKRN3* mutation rate of 3.8% (67/1,758) in NSCLC samples (n = 1,758; Table S1), which included nonsense mutations, frameshift deletions, frameshift insertions, splice mutations, missense mutations, and genomic deletions (Fig. 1 B and Table S1). Across all 1,758 NSCLC samples, nonsense mutations, frameshift deletions, frameshift insertions, splice mutations, and deletions accounted for 45% of genomic alterations in *MKRN3* (Fig. 1 B and Table S1), with 55% of mutations being missense, around 58% of which were classed as disruptive by both SIFT and PolyPhen-2 software tools that predict the functional effects of nonsynonymous protein coding single nucleotide polymorphisms (Fig. 1 B and Table S1; Adzhubei et al., 2010). We further provided evidence to show that the missense mutations are loss-of-functional (see below, Fig. 5 D). *MKRN3* is maternally imprinted, and the paternal allele is expressed (Abreu et al., 2013). We extended the mutations analysis to the intragenic mutation of *MKRN3* in the NSCLC cell line in which it was possible to compare the nucleotide sequence of PCR products generated from genomic DNA or cDNA. Although the *MKRN3* mutation was heterozygous in genomic DNA, only the mutant sequence was detected in the lung cancer cell–derived transcripts, consistent with monoallelic expression of the mutant copy from the non-imprinted allele (Fig. S1 B).

It has been reported that *MKRN3* is expressed in the hypothalamic arcuate nucleus of mice during postnatal development (Abreu et al., 2013). We demonstrated that *MKRN3* is also expressed in both mouse and human lung tissues (Fig. 1 C). *MKRN3* inactivation was found across all lung cancer stage subtypes, including early-stage (stage I and II) lung cancer, suggesting that genomic *MKRN3* alterations can arise around disease initiation (Table S1). To explore a possible role of MKRN3 in lung cancer, we assessed MKRN3 expression in humans with lung cancer. As shown in Fig. 1, D–F; Fig. S1 D; and Table S2, immunohistochemistry staining and Western blotting analysis revealed that the levels of MKRN3 protein were decreased in the tumor samples as compared with the adjacent normal counterparts. Immunohistochemistry staining and Western blots on a panel of human lung cancer cell lines demonstrate that MKRN3 is expressed in lung cancer cells (Fig. 1 D and Fig. S2 A). The identification of MKRN3 inactivation in TCGA patients and Asian patients shows that the MKRN3 inactivation in lung cancer is generalizable and is not restricted to a specific ethnic group. Although *MKRN3* is a maternally imprinted gene, there are no gender differences in *MKRN3* mutations ($P = 0.922$, Fisher's test) and expression ($P = 0.673$, Fisher's test). Strikingly, lower MKRN3 expression is associated with a significantly shorter overall survival time in two separate lung cancer patient cohorts (Fig. 1 G). As indicated by the hazard ratios, MKRN3 expression levels serve as an independent predictor for risk stratification of overall survival and relapse-free survival in patients (Fig. 1 G). Together, these findings highlight MKRN3 as a potential biomarker for lung cancer and suggest a role of genomic *MKRN3* inactivation in lung tumorigenesis.

Functional validation of *MKRN3* as a tumor suppressor gene in NSCLC

The biological function of MKRN3 was investigated using various human NSCLC models. MKRN3 biological function was evaluated by reexpressing MKRN3 in *MKRN3*-inactivated NSCLC cells. A human NSCLC cell line (H1703, lung squamous cell carcinoma) was identified to contain a *MKRN3* frameshift deletion (c.636_636delC, p.Y212Yfs*73; Ghandi et al., 2019; Fig. S1 B). Lentivirus-mediated *MKRN3* transduction into *MKRN3*-inactivated H1703 cells induced MKRN3 expression (Fig. 2 B and Fig. S2 A).

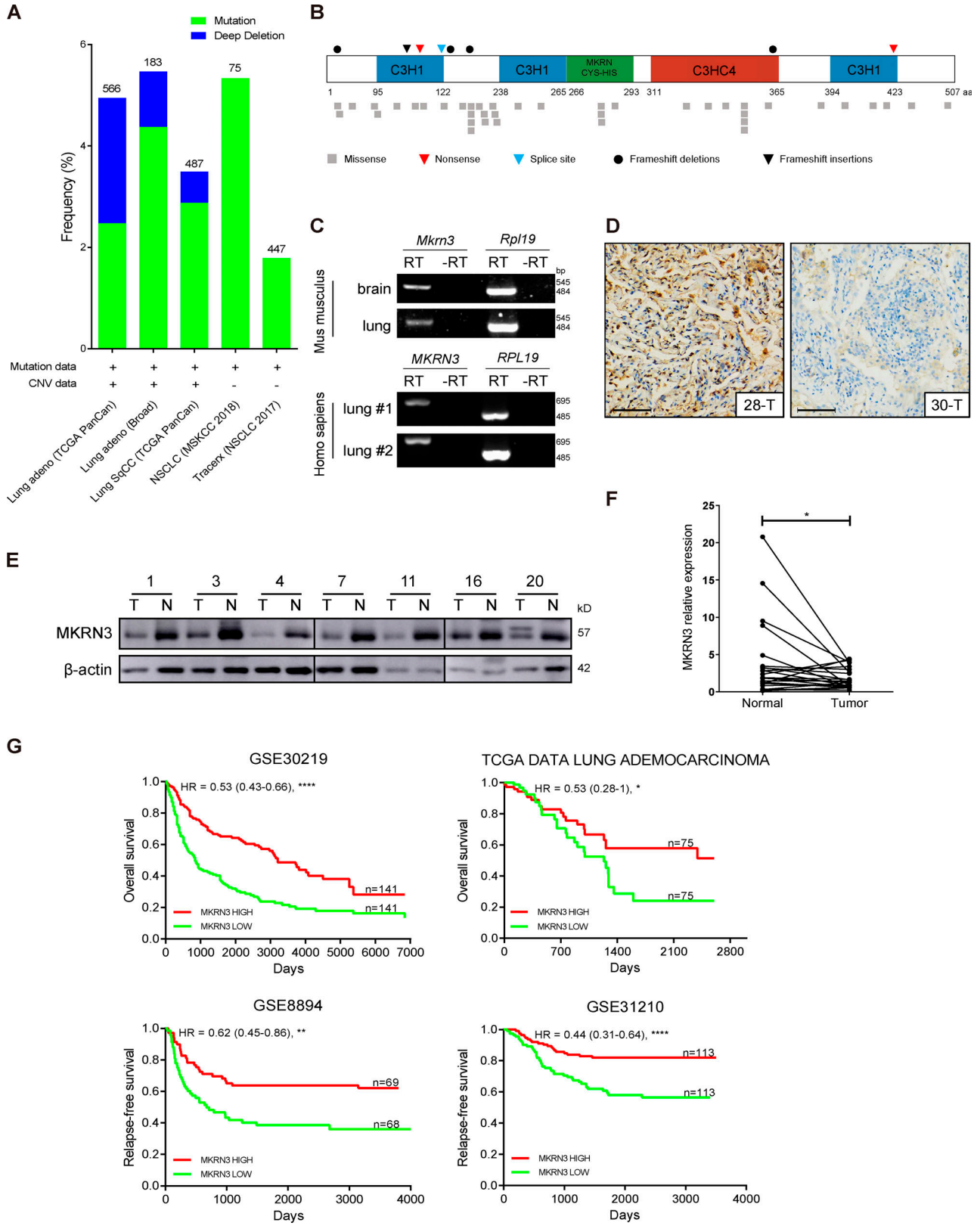

Figure 1. **Identification and clinical significance of genomic *MKRN3* aberrations in human NSCLCs. (A)** Frequency of genomic *MKRN3* aberrations in five NSCLC cohorts. The mutation type is indicated. The total number of genomes analyzed in each cohort is shown above each column. Lung adeno, lung adenocarcinoma; Lung SqCC, lung squamous cell carcinoma; CNV, copy number variants. **(B)** Predicted consequences of *MKRN3* mutations identified from the analysis of 1,828 human lung cancer genomes are depicted across the MKRN3 protein (NCBI, NP_005655.1). MKRN3 protein domains are highlighted: three C3H motifs (blue), one C3HC4 RING motif (red), and one MKRN-specific Cys-His domain (green). The numbers correspond to the amino acid positions in the protein. Mutation type is indicated. **(C)** RT-PCR demonstrates MKRN3 expression in both mouse and human lung tissues. RPL19 was included as a loading

control. -RT indicates samples treated without RT. *MKRN3* is an intronless gene. Therefore, a DNase treatment was performed on the RNA samples to digest all the possibly contaminating genomic DNA. **(D)** MKRN3 immunohistochemistry staining in the lung cancer samples. 28-T and 30-T denote two lung cancer samples from case #28 and #30 as indicated in Table S2. Left: Positive. Right: Negative. Scale bar, 80 µm. **(E)** Decreased MKRN3 protein expression in seven representative lung tumor samples. T, lung tumor samples; N, paired adjacent normal tissues. **(F)** MKRN3 protein levels in 24 lung tumor samples (T) and their paired adjacent normal tissues (N; *, P = 0.0447, paired *t* test). Quantification of Western blotting bands in Fig. S4 B. **(G)** Kaplan–Meier survival curves for overall survival and disease relapse-free survival stratified by MKRN3 expression levels using the GEO accession nos. GSE30219 (****, P = 7.77e-09, hazard ratio [HR] = 0.53 [0.43–0.66, 95% confidence interval (CI)]), GSE8894 (**, P = 0.0045, HR = 0.62 [0.45–0.86, 95% CI]), GSE31210 (****, P = 1.97e-05, HR = 0.44 [0.31–0.64, 95% CI]), and TCGA (*, P = 0.049, HR = 0.53 [0.28–1, 95% CI]) lung adenocarcinoma dataset (P values by log-rank test). All panels represent data from two or three independent experiments.

MKRN3 reexpression reduced the number of viable cells (Fig. 2 A) and proliferative properties (Fig. 2, B and C), but increased cell apoptosis (Fig. S2, C and D). MKRN3 restoration also decreased the cell cycle, increasing the proportion of cells in G2/M phase (Fig. 2 D). MKRN3 reexpression inhibited anchorage-independent growth in *MKRN3*-inactivated lung cancer cells (Fig. 2 E). To determine whether the inhibition of cell proliferation is manifested in vivo, we generated both control and MKRN3-restored H1703 xenografts in nude mice. MKRN3 restoration markedly attenuated tumor growth (Fig. 2, F and G). To further test the role of MKRN3 in lung cancer, we extended these findings to a second NSCLC cell line (H1437, lung adenocarcinoma) with MKRN3 inactivation (Fig. S2 A). Consistent with the above data, MKRN3 reexpression reduced the cell growth and proliferation in vitro and in vivo (Figs. 2 and S3). Collectively, these results demonstrate that MKRN3 inactivation promotes lung cancer tumorigenesis.

MKRN3 KO mice are susceptible to urethane-induced NSCLC

The incidence of cancer has been observed to increase markedly in tumor suppressor–deficient mice upon exposure to environmental insult. We speculated that inactivation of *MKRN3* might also render mice susceptible to a second cancer trigger. To test this hypothesis, we challenged *Mkrn3* KO (Li et al., 2020) and control littermates with urethane, a DNA alkylating agent that is classified as a chemical carcinogen and is widely used to induce lung tumor formation in mice (McLoed et al., 2016; Rex et al., 2016; To et al., 2008; Fig. 3 A and Fig. S4 B). Consistent with previous reports (McLoed et al., 2016), injections of urethane resulted in a very low incidence of lung tumors from mice with WT genotypes (Fig. 3, B and C). Only a low percentage of WT mice developed lung tumors (Fig. 3, B–D). Notably, almost all *Mkrn3* KO ($Mkrn3^{p-/m+}$) mice developed large and rapidly growing lung tumors in response to urethane (Fig. 3, B, D, and E). Within the same mice, multifocal lung tumor development was observed, suggesting multiple transformation events (Fig. 3, B and C). Tumors were histologically classified as adenocarcinomas (Fig. 3 C). During the observation period, we did not observe metastatic spread of these primary lung tumors. Our results show that loss of MKRN3 renders mice susceptible to urethane-induced lung cancer.

Lung cell–specific KO of *MKRN3* accelerates NSCLC tumorigenesis in mice

MKRN3 genomic alterations are enriched in human lung cancer samples harboring oncogenic *KRAS* mutations (Fig. S1 A and Table 1). To genetically validate the synergistic effect of the two

Table 1. **Genomic MKRN3 aberrations with KRAS mutations in human NSCLCs**

Sample ID	Cancer type	Stage	*MKRN3*	*KRAS*
nsclc_mskcc_2018s51	NSCLC	NA	R102Kfs*28	G13C
LUAD-RT-S01777	Lung adenocarcinoma	IIIB	P362Hfs*34	G12A
TCGA-62-8398-01	Lung adenocarcinoma	IIIA	S118L	G12D
LUAD-NYU408	Lung adenocarcinoma	IB	A203G	G12V
nsclc_mskcc_2018s26	NSCLC	NA	Q281K	G12C
TCGA-78-7166-01	Lung adenocarcinoma	IIB	W347C	G12C
TCGA-O2-A52Q-01	Lung squamous cell carcinoma	III	R401W	G13C
TCGA-64-5775-01	Lung adenocarcinoma	IIIA	P411Q	Q61L
LUAD-S00488	Lung adenocarcinoma	IIIA	Hom Del	G12C
TCGA-44-8117-01	Lung adenocarcinoma	IB	Hom Del	L19F
TCGA-64-1677-01	Lung adenocarcinoma	IIIA	Hom Del	G12C
TCGA-86-7953-01	Lung adenocarcinoma	IA	Hom Del	G12D
TCGA-95-7039-01	Lung adenocarcinoma	IIB	Hom Del	D33E
TCGA-95-A4VP-01	Lung adenocarcinoma	IIIA	Hom Del	G12V

The co-occurrence of *MKRN3* aberrations with *KRAS* mutations in human lung cancer datasets. Data from lung cancer patients obtained from TCGA lung cancer studies. Sample IDs as well as the precise mutations identified in these patients are indicated. Hom del, homozygous deletion; NA, not available.

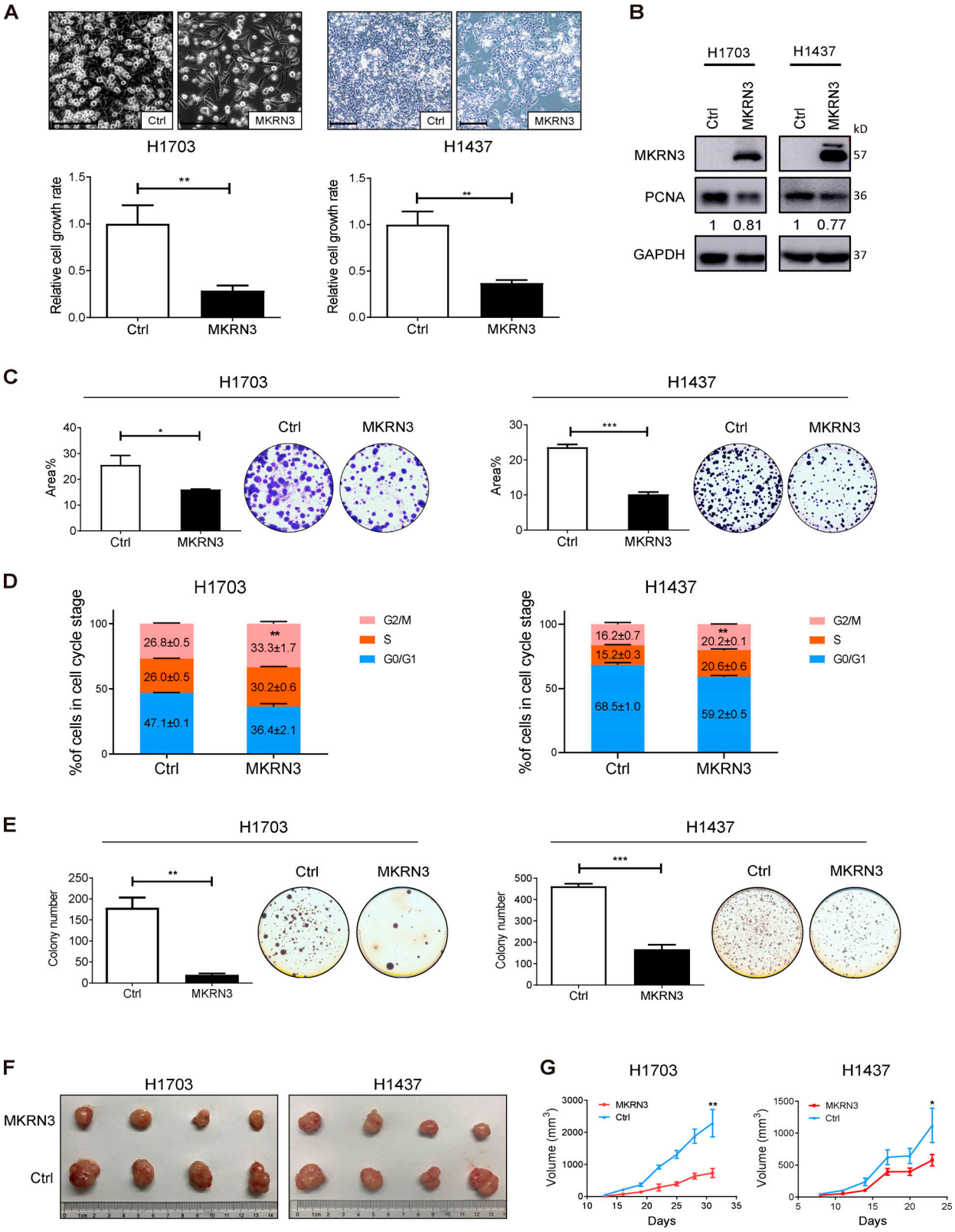

Figure 2. **Reconstitution of MKRN3 inhibits tumor growth and proliferation in *MKRN3*-inactivated NSCLCs. (A)** Lentivirus-mediated MKRN3 restoration reduces the viability of H1703 (lung squamous cell carcinoma) and H1437 (lung adenocarcinoma) cells, as assessed by representative bright field microscopy images (top, scale bar, 200 µm) and by CellTiter-Glo viability assay (bottom; $n = 3$ per group; **, $P < 0.01$; unpaired t test). **(B)** Western blotting with proliferating cell nuclear antigen (PCNA) antibody demonstrates that MKRN3 restoration represses cell proliferation. **(C)** Crystal violet staining assays show that MKRN3 restoration suppresses lung cancer proliferation of H1703 and H1437 cells. Representative plates (right) and mean colony numbers (left) are shown (± SEM; $n = 3$ per group; *, $P < 0.05$; ***, $P < 0.001$; unpaired t test). **(D)** Cell-cycle analyses demonstrating that MKRN3 restoration decreases the cell cycle in both

H1703 and H1437, increasing the proportion of cells in G2/M phase (n = 3 per group; **, P < 0.01; unpaired t test). **(E)** MKRN3 restoration suppresses anchorage-independent growth of H1703 and H1437 cells. Representative plates (right) and mean colony numbers (left) are shown (± SEM; n = 3 per group; **, P < 0.01; ***, P < 0.001; unpaired t test). **(F and G)** MKRN3 restoration inhibits the growth of H1703 and H1437 xenografts in nude mice. Growth curves (G) and representative photo images (F) of transplanted tumors are shown. Error bars are the mean ± SEM of four replicates (*, P < 0.05; **, P < 0.01; unpaired t test). All panels represent data from two or three independent experiments. Ctrl, control.

alterations in the lung tumors studied here, we performed mouse studies. The commonly used *K-ras*$^{LSL\text{-}G12D/+}$ (K) mouse model harbors Cre-inducible alleles of *K-ras* gene and develops lung tumors. To enable inducible deletion of *Mkrn3* specifically in lung cells, mice with a floxed *Mkrn3* exon 1 allele were generated. We combined the *Mkrn3*$^{pfl/m+}$ alleles with K mouse and targeted Cre expression to the lungs (Fig. S4, C and D) using intranasal adenovirus delivery (DuPage et al., 2009; Xie et al., 2018; Fig. 4 A).

Next, cohorts of Ad-Cre–infected *K-ras*$^{LSL\text{-}G12D/+}$ (K) and *K-ras*$^{LSL\text{-}G12D/+}$; *Mkrn3*$^{pfl/m+}$ (KM) mice were followed over time. The KM mice showed earlier onset and a more rapid progression of the alveolar lesions. Histopathological analysis of their lungs at 12 mo after Ad-Cre infection revealed a significant increase in tumor burden compared with that in K controls (Fig. 4, B–E). Moreover, KM mice displayed advanced adenocarcinomas, a tumor stage that is extremely infrequent at this time in tumors driven by *K-rasG12D* alone (Fig. 4, B–E). To quantify the extent of progression of KM tumors, we devised a grading system by which to evaluate the stage of every tumor in each mouse as previously described (Jackson et al., 2005). Using this grading scheme, we confirmed that MKRN3 inactivation resulted in a markedly more severe tumor phenotype in KM mice (Fig. 4 E and Fig. S4 E). KM mice developed lung adenocarcinomas, identified by positive staining for TTF1^{+} (immunostaining biomarker for adenocarcinoma) and negative staining for p40 (immunostaining biomarker for squamous cell carcinomas; Yatabe et al., 2019; Fig. 4 F). Altogether, these observations demonstrate that *MKRN3* inactivation in the presence of *K-ras* (G12D) mutations accelerated lung tumor progression.

MKRN3 interacts with and ubiquitinates PABPC1

What are the molecular mechanisms underlying MKRN3 tumor suppression? MKRN3 is a ubiquitin (Ub) E3 ligase that facilitates the ubiquitination of target proteins (Abreu et al., 2013; Li et al., 2021; Li et al., 2020). To identify the potential substrates for MKRN3 in the cancer context, Flag-tagged MKRN3 was transduced into MKRN3-inactivated H1703 lung cancer cells as bait. MKRN3 was recovered along with proteins that potentially formed complexes with MKRN3 through coimmunoprecipitation with anti-Flag beads, and the samples were subjected to mass spectrometry–based proteomics screening. As shown in Fig. 5 A, PABPC1 protein emerged as the hit with the highest confidence. The interaction between endogenous PABPC1 and restored Flag-MKRN3 was validated in H1703 cells (Fig. 5 B) and was further confirmed in an additional human lung adenocarcinoma cell line H1437 (Fig. 5 B).

We next sought to determine whether MKRN3 ubiquitinates PABPC1 and whether cancer-derived mutations in *MKRN3* alter its Ub ligase activity. We started with an assay in HEK293T cells to measure the ubiquitination function of MKRN3. MKRN3 was found to interact with and ubiquitinate ectopically expressed PABPC1 in the HEK293T model (Fig. 5 C and Fig. S5 A) and significantly increase the ubiquitination of the endogenous PABPC1 in lung cancer cells (Fig. 5 E). *MKRN3* missense mutations identified in NSCLC patients were found to substantially compromise MKRN3-mediated PABPC1 ubiquitination (Fig. 5 D).

Previous studies showed that several proteins interact with PABPC1 via PABP-interacting motif 2 (PAM2; Xie et al., 2014), which contained a conserved peptide sequence xxLNxxAxEFxPxxx (Fig. 5 F). Thus, we speculated that MKRN3 interacts with PABPC1 via PAM2 at amino acid positions 197–211. To define the sites in MKRN3 that are responsible for recognizing PABPC1, we cotransfected HEK293T cells with Flag-PABPC1 and either WT or mutant MKRN3 (A203S, F206A, P208A, A203S/F206A, or A203S/F206A/P208A). Flag-PABPC1 coimmunoprecipitation showed that WT, MKRN3^{A203S}, and MKRN3^{P208A} had equivalent interactions with PABPC1, while the interaction between MKRN3^{F206A} and PABPC1 was significantly impaired (Fig. 5 G). Furthermore, MKRN3$^{A203S/F206A}$ and MKRN3$^{A203S/F206A/P208A}$ exerted weaker interactions with PABPC1 than WT MKRN3 (Fig. 5 G). Strikingly, MKRN3$^{A203S/F206A/P208A}$ decreased the ubiquitination of the PABPC1 protein (Fig. 5 G) and attenuated MKRN3 tumor suppression properties in lung cancer cells (Fig. 5, H and I). Overall, these results illustrate that MKRN3 directly interacts with PABPC1, and the A203/F206/P208 of MKRN3 are crucial interaction residues mediating PABPC1 ubiquitination.

MKRN3 modulates NSCLC cell proliferation largely through PABPC1 ubiquitination

Interestingly, MKRN3-mediated ubiquitination of PABPC1 seemed to have no effect on the stability of PABPC1 (Fig. 5 B). Transfection of MKRN3 in HEK293T cells resulted in increased PABPC1 ubiquitination in the presence of WT Ub or Ub that only forms K63 linkages (UbK63), one type of poly-Ub chains that typically leads to signal transduction (Komander and Rape, 2012; Kwon and Ciechanover, 2017), compared with HEK293T cells transfected with empty vector (Fig. 6 A). In contrast, the expression of MKRN3 together with Ub that only forms K48 linkages (UbK48), one type of poly-Ub chains that typically leads to protein degradation (Komander and Rape, 2012; Kwon and Ciechanover, 2017), did not result in PABPC1 ubiquitination in HEK293T cells (Fig. 6 A). In addition, a cycloheximide chase experiment also showed that compared with MKRN3-C258*, MKRN3 did not induce PABPC1 degradation in H1703 cells (Fig. 6 B).

To further elucidate the molecular mechanisms underlying MKRN3-mediated ubiquitination of PABPC1, we found that the second RNA recognition motif (RRM) in PABPC1 was required for PABPC1 ubiquitination (Fig. 6 C and Fig. S5 B). We then

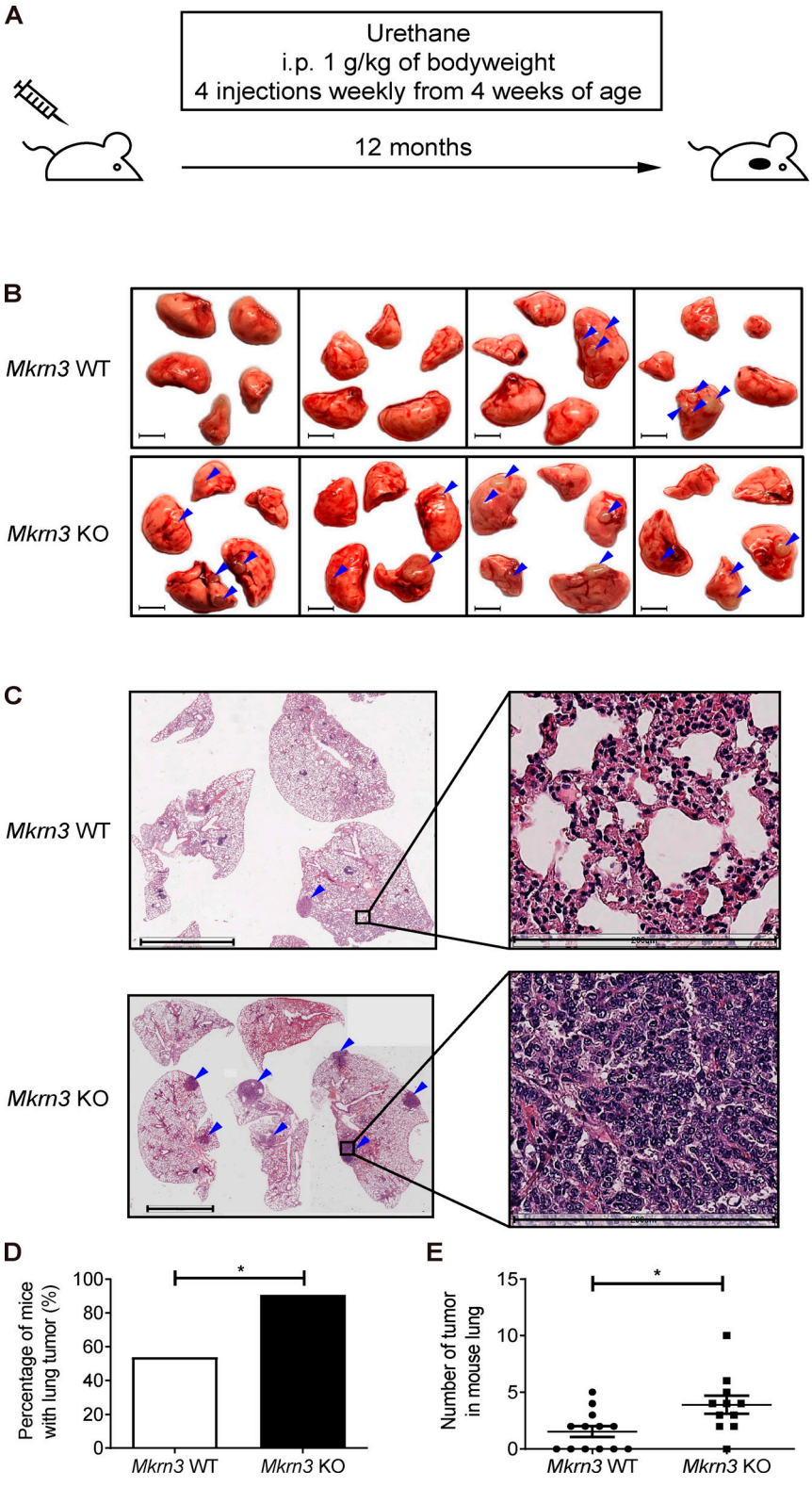

Figure 3. **MKRN3 KO mice are susceptible to urethane-induced lung cancer. (A)** Diagram of the experimental procedure. *MKRN3* WT and KO mice were given four injections of urethane (1 g/kg of bodyweight; i.p.) weekly from 4 wk of age. All mice were littermates. **(B)** Four representative cases of lung tumors from *MKRN3* WT and KO mice are shown 12 mo after the last injection. Blue arrows indicate tumors. Scale bars, 5 mm. **(C)** Representative histology of lung tumors in *MKRN3* WT and KO mice. Top: Normal lung from a urethane-treated *MKRN3* WT mouse. Bottom: Lung adenocarcinoma from a urethane-treated *MKRN3* KO mouse. All images are from H&E-stained sections. Scale bars, 4 mm (left) and 200 µm (right). **(D)** Lung cancer incidence (*, $P < 0.05$; χ^2 test). **(E)** Tumor number per mouse lung (*, $P < 0.05$; unpaired t test). Data are summarized from 13 *MKRN3* WT and 11 *MKRN3* KO mice at 12 mo after the last injection of urethane.

mutated the eight lysine residues individually in RRM2. Our strategy was to mutate these putatively ubiquitinated lysines to arginines, since arginine cannot be ubiquitinated but retains the positive charge. Single mutations of K104R, K108R, K113R, K129R, K138R, K157R, and K174R showed reductions in the overall level of PABPC1 ubiquitination (Fig. 6 D). The double mutant (K104R/K108R; 2KR), triple mutant (K104R/K108R/K113R; 3KR), quadruple mutant (K104R/K108R/K113R/K129R; 4KR), 5KR mutant (K104R/K108R/K113R/K129R/K138R), 6KR mutant (K104R/K108R/K113R/K129R/K138R/K157R), and 7KR mutant (K104R/K108R/K113R/K129R/K138R/K157R/K174R) were then constructed. PABPC1 ubiquitination was at the lowest level detected in this

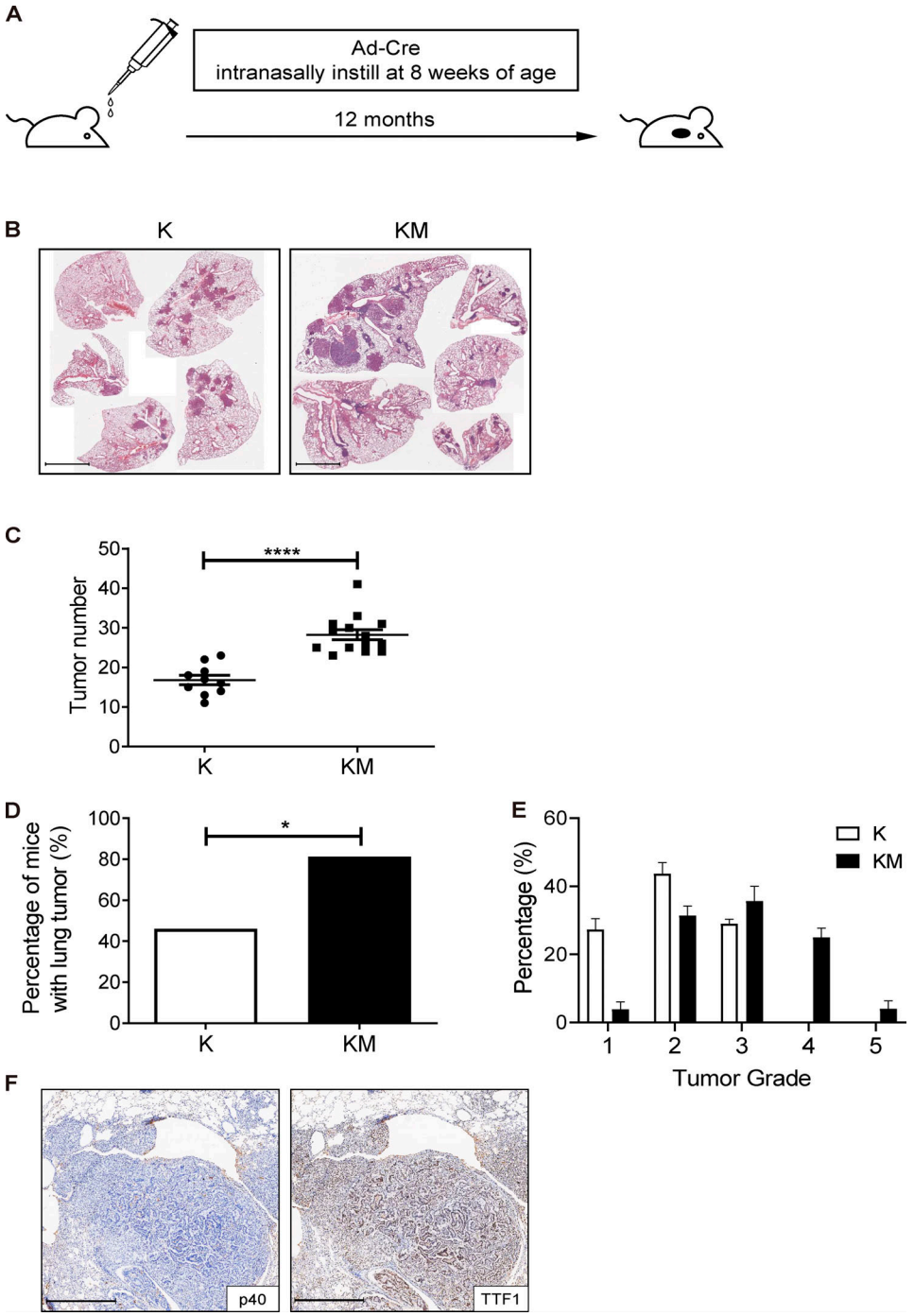

Figure 4. **Lung cell–specific KO MKRN3 accelerates NSCLC tumorigenesis in mice. (A)** Diagram of the experimental procedure. *K-ras*$^{LSL\text{-}G12D/+}$ (K), *K-ras*$^{LSL\text{-}G12D/+}$; *Mkrn3*$^{pfl/m+}$ (KM) mice were intranasally instilled with Ad-Cre at 8 wk of age. All mice were littermates. **(B)** Representative H&E staining of paraffin-embedded lung sections obtained from *K-ras*$^{LSL\text{-}G12D/+}$ (K), *K-ras*$^{LSL\text{-}G12D/+}$; *Mkrn3*$^{pfl/m+}$ (KM) mice 12 mo after Ad-Cre infection. Scale bars, 4 mm. **(C)** Lung cancer incidence from *K-ras*$^{LSL\text{-}G12D/+}$ (K), *K-ras*$^{LSL\text{-}G12D/+}$; *Mkrn3*$^{pfl/m+}$ (KM) mice 12 mo after Ad-Cre infection (*, $P < 0.05$; χ^2 test). **(D)** Tumor number per mouse lung from *K-ras*$^{LSL\text{-}G12D/+}$ (K), *K-ras*$^{LSL\text{-}G12D/+}$; *Mkrn3*$^{pfl/m+}$ (KM) mice 12 mo after Ad-Cre infection (****, $P < 0.0001$; unpaired *t* test). **(E)** Tumor grade percentage from *K-ras*$^{LSL\text{-}G12D/+}$ (K), *K-ras*$^{LSL\text{-}G12D/+}$; *Mkrn3*$^{pfl/m+}$ (KM) mice 12 mo after Ad-Cre infection. **(F)** Representative immunostaining of paraffin-embedded sections showing tumors from Ad-Cre–infected *K-ras*$^{LSL\text{-}G12D/+}$; *Mkrn3*$^{pfl/m+}$ (KM) mice using antibodies against p40 and TFF1. Scale bar, 700 µm. The data were summarized from 168 tumors in 10 K (*K-ras*$^{LSL\text{-}G12D/+}$) mice and 396 tumors in 14 KM mice.

7KR mutant (Fig. 6 E), indicating that all seven lysines are subject to PABPC1 ubiquitination. Interestingly, these seven lysine residues are conserved across human, rabbit, rat, mouse, zebrafish, and frog (Fig. S5 C).

To determine whether MKRN3 acts as a tumor suppressor by mediating ubiquitination of PABPC1, a series of rescue experiments was performed in a lung cancer context. Endogenous PABPC1 was knocked out in H1703 cells with a CRISPR/Cas9

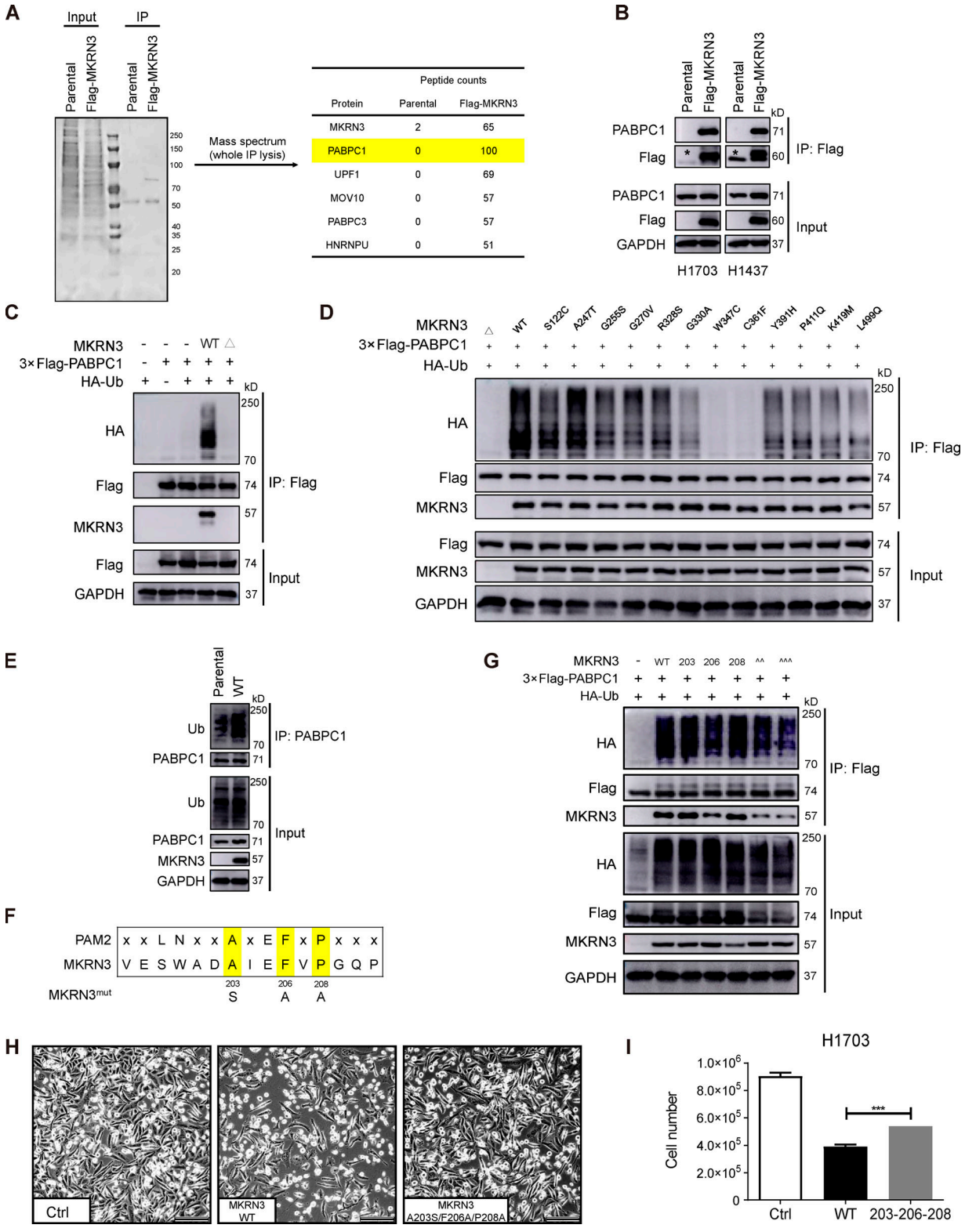

Figure 5. **MKRN3 interacts with and ubiquitinates PABPC1. (A)** Identification of MKRN3-interacting proteins through coimmunoprecipitation followed by mass spectrometry–based proteomics showing that PABPC1 was the most abundant binding protein. MKRN3 inactivated lung cancer H1703 cells were restored with Flag-MKRN3, and a pull-down assay was performed using anti-Flag antibody. Pull-down samples were detected by SDS-PAGE and followed by Coomassie staining. The table shows high-confidence hits in the mass spectrum. **(B)** Endogenous PABPC1 interacts strongly with MKRN3 in H1703 and H1437 lung cancer cells. The H1703 and H1437 cells were transduced by Flag-MKRN3, and cell lysates were subjected to a coimmunoprecipitation assay using anti-Flag antibody, followed by immunoblotting with anti-PABPC1 or anti-Flag antibody. Asterisk indicates heavy chain of IgG. **(C)** MKRN3 ubiquitinates PABPC1. Flag-tagged PABPC1 was efficiently ubiquitinated by exogenous WT MKRN3. Lung cancer–derived truncating mutant (MKRN3 C258*, indicated by Δ) compromises the ubiquitination activity. HEK293T cells were cotransfected with the indicated plasmids, and cell lysates were immunoprecipitated with anti-Flag

antibody, followed by immunoblotting with anti-HA antibody to detect ubiquitinated PABPC1. **(D)** *MKRN3* missense mutations identified in lung cancer patients disrupt MKRN3-mediated PABPC1 ubiquitination. **(E)** Flag-MKRN3 restoration increases the ubiquitination of endogenous PABPC1 in H1703 lung cancer cells. Endogenous PABPC1 protein was immunoprecipitated using anti-PABPC1 antibody, followed by immunoblotting with anti-Ub or other indicated antibodies. **(F)** MKRN3 amino acids 197–211 are aligned with the PAM2 amino acid sequence. **(G)** MKRN3 directly interacts with PABPC1, and the A203/F206/P208 of MKRN3 are crucial interaction residues mediating PABPC1 ubiquitination. HEK293T cells were cotransfected with indicated plasmids, and cell lysates were immunoprecipitated with anti-Flag antibody, followed by immunoblotting for MKRN3 to detect the interaction between MKRN3 and PABPC1 or with anti-HA antibody to detect ubiquitinated PABPC1. ^^, $MKRN3^{A203S\text{-}F206A}$; ^^^, $MKRN3^{A203S\text{-}F206A\text{-}P208A}$. **(H and I)** $MKRN3^{A203S\text{-}F206A\text{-}P208A}$ mutant attenuates MKRN3 tumor suppression properties in H1703 lung cancer cells, as assessed by representative bright field microscopy images (H) and by cell counting (I; $n = 3$ per group; ***, $P < 0.001$; unpaired t test). Scale bar, 200 µm. All panels represent data from two or three independent experiments. Ctrl, control.

approach, followed by reconstitution of WT or 7KR mutant PABPC1 (Fig. 6 F). In this MKRN3-inactivated lung cancer context, MKRN3 restoration promoted ubiquitination of WT PABPC1 and exhibited tumor suppression properties, while enforced MKRN3 expression in PABPC1 mutant lung cancer cells attenuated various MKRN3 tumor suppression properties (Fig. 6, G and H). These data show that MKRN3 functions as a tumor suppressor in lung cancer largely through PABPC1 ubiquitination.

MKRN3-PABPC1 axis regulates global protein synthesis to control cell proliferation in NSCLC

PABPC1 is one of the 1,000+ RNA-binding proteins found in humans (Xie et al., 2014). Previous studies established that PABPC1 and eIF4G are direct interacting components in the translation initiation complex (TIC), and the PABPC1-eIF4G interaction is important for both the TIC formation and overall mRNA translation efficiency (Tritschler et al., 2010; Xie et al., 2014). Then we explored whether MKRN3 affects the interaction between PABPC1 and eIF4G. As shown in Fig. 7 A, the same amounts of antibody enriched almost equal PABPC1 proteins in both groups, while less eIF4G was present in the MKRN3-restored group. Therefore, MKRN3 restoration hinders the formation of PABPC1-eIF4G complex.

We next evaluated whether MKRN3 inactivation can affect global protein translation. Protein synthesis is globally repressed in MKRN3 restored lung cancer cells as measured by L-azidohomoalanine (L-AHA) incorporation (Fig. 7 B). Since MKRN3 restoration induced cell cycle arrest in G2/M phase (Fig. 2 D), we investigated transcription and expression level of *CCNB1*, which is a cell cycle regulator of G2/M phase. We found that PABPC1 does bind to the 3′ poly(A) tail of *CCNB1* mRNA in the lung cancer context (Fig. 7 C). *CCNB1* encodes cyclin B1, which functions as a cell-cycle regulator, and its overexpression has been shown to correlate with tumor progression (Fang et al., 2014). With the particular interest in the homeostasis of *CCNB1* mRNAs, then we asked whether MRKN3-mediated PABPC1 ubiquitination would have any effect on their binding to the poly(A) tail of *CCNB1* mRNA. As shown in Fig. 7 D, RNA immunoprecipitation (IP) assay indicated that the same amounts of anti-Flag (pulling down Flag-PABPC1 protein) did pull down significantly less *CCNB1* mRNAs in MKRN3-restored lung cancer cells (Fig. 7 D). Down-regulation of cyclin B1 by MKRN3-PABPC1 was further validated at the protein level (Fig. 7 E) but not the mRNA level (Table S3).

All these data demonstrated that the ubiquitination of PABPC1 by MKRN3 attenuates its binding to 3′ poly(A) tails of mRNAs, and decreases the TIC formation, thereby repressing global protein synthesis and maintaining lung cancer cells with limited proliferative capacity (Fig. 7 F). In contrast, inactivated MKRN3 reduces PABPC1 ubiquitination, promotes its binding to 3′ poly(A) tails of mRNAs, and thereby accelerates global protein synthesis and promotes lung cancer proliferation and progression (Fig. 7 F).

Discussion

The molecular mechanism underlying the progression of NSCLC is not fully understood. Our findings of recurrent genomic alterations, together with various functional, mouse model, and mechanistic data herein, highlight the *MKRN3* gene as a bona fide tumor suppressor gene contributing to NSCLC progression. Inactivated MKRN3 is unable to ubiquitinate PABPC1 and leads to an increase in the global translation rate and altered pattern of mRNA translation, thereby contributing to the tumor proliferation and progression. We believe our findings have important implications for understanding the molecular events shaping oncogenesis in NSCLC and for elucidating the genetic drivers of PABPC1 ubiquitination. A deep understanding of the mechanisms underlying E3 ligase regulation and function in tumorigenesis is expected to identify novel prognostic markers and to enable the development of the next generation of anticancer therapies (Hyer et al., 2018; Kim et al., 2017; Popovic et al., 2014; Senft et al., 2018).

It is intriguing that *MKRN3* inactivating mutations are so frequent in NSCLC given that MKRN3 is ubiquitously expressed (Fig. S4 A). Certainly this is one limitation of our results. Nonetheless, our results indicate that the MKRN3-PABPC1 pathway plays a prominent role in lung cancer pathogenesis. It is also striking that humans with germline *MKRN3* mutations only develop an overt pathology within the neuroendocrine brain that ultimately regulates the reproductive axis, a disease called CPP (Abreu et al., 2013; Latronico et al., 2016; Shin, 2016). From a pathophysiologic standpoint, it seems that inactivation of certain genes, such as *MKRN3*, leads to distinct physiological outcomes depending on the cellular context. Indeed, we previously demonstrated that the *DMD* and *DEPDC5* genes function as tumor suppressors (Pang et al., 2019; Wang et al., 2014), but their germline mutations result in muscular dystrophy and focal epilepsy, respectively (Hoffman et al., 1987; Ishida et al., 2013). Notably, cohorts of individuals with CPP show an increased risk of malignancies such as lung cancers (Ben Khedher et al., 2017; Calcaterra et al., 2013; Kreuzer et al., 2003). It is hard to imagine that two entirely different classes of disease, such as lung cancer and CPP, can converge at a critical point

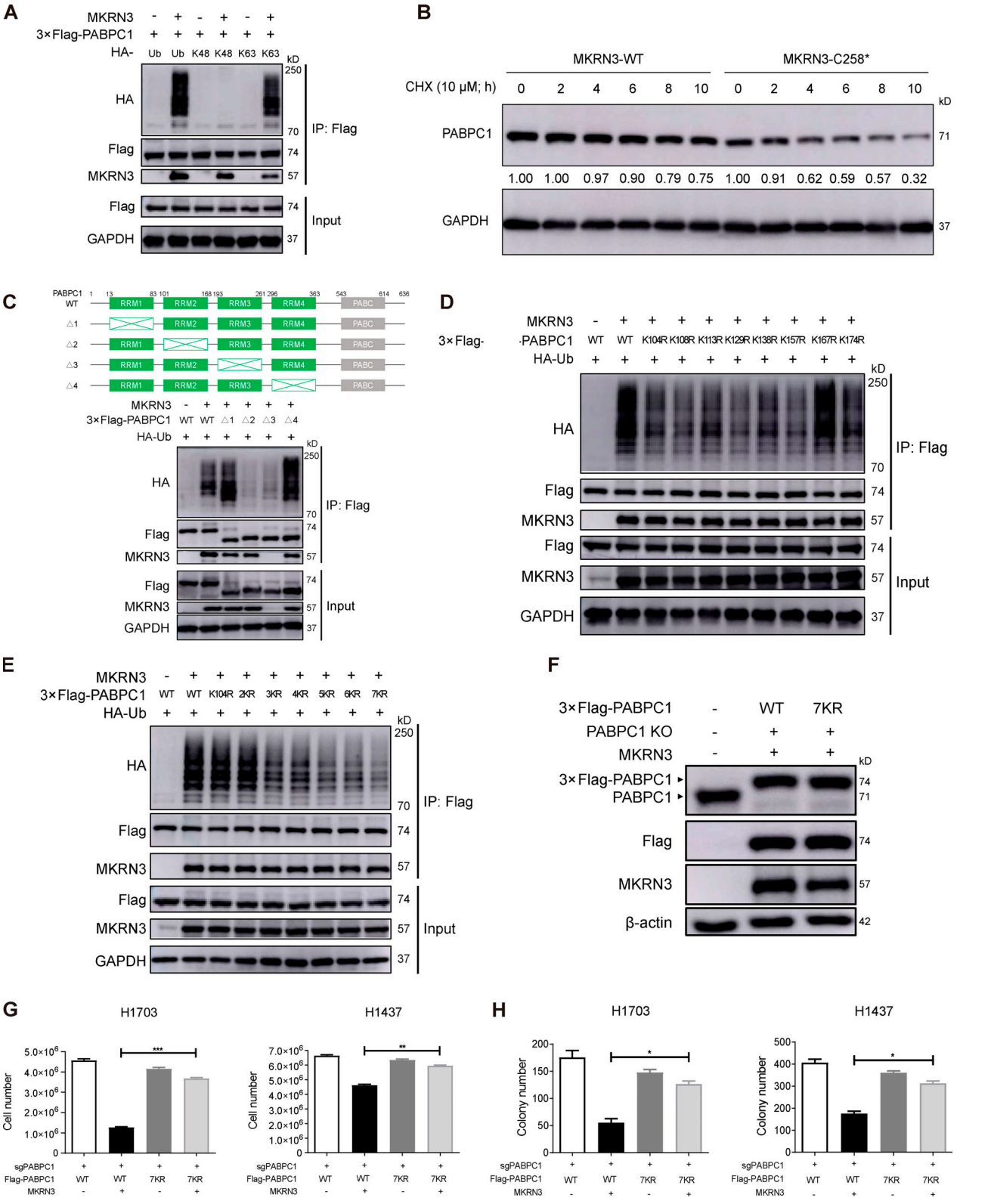

Figure 6. **MKRN3 functions as a tumor suppressor largely through PABPC1 ubiquitination. (A)** MKRN3 promotes K63-linked polyubiquitination of PABPC1. HEK293T cells transfected with MKRN3, Flag-PABPC1, and either WT HA-Ub or mutant Ub that form only K63 (UbK63) or K48 (UbK48) linkages were immunoblotted for the indicated proteins on immunoprecipitated Flag-PABPC1. **(B)** MKRN3 does not induce PABPC1 degradation. H1703 cells were infected with MKRN3 or MKRN3-C258* lentivirus and treated with cycloheximide at 10 μM subsequently. Cells were harvested at indicated time and immunoblotted for PABPC1 and GAPDH. CHX, cycloheximide. **(C)** The second RRM in PABPC1 is required for MKRN3-mediated PABPC1 ubiquitination. A diagram shows domain structures of PABPC1 (top). The location of each domain was indicated at the bottom. HEK293T cells transfected with MKRN3, Flag-PABPC1 (WT or PABPC1 variants: Δ1, Flag-PABPC1-ΔRRM1; Δ2, Flag-PABPC1-ΔRRM2; Δ3, Flag-PABPC1-ΔRRM3; Δ4, Flag-PABPC1-ΔRRM4), and WT HA-Ub were immunoblotted for the

indicated proteins on immunoprecipitated Flag-PABPC1. Flag-PABPC1-ΔRRM3 and MKRN3 cotransfection results in MKRN3 down-regulation and attenuates PABPC1 ubiquitination. The 10 lysine residues (K196, K208, K213, K221, K229, K231, K246, K254, K259, and K268) in RRM3 are not subject to ubiquitination by MKRN3 (Fig. S4 B). **(D and E)** PABPC1 ubiquitination by MKRN3 primarily occurs at seven lysine residues (K104, K108, K113, K129, K138, K157, and K174) in RRM2. HEK293T cells transfected with MKRN3, Flag-PABPC1 (WT or indicated K-to-R point mutants), and WT HA-Ub were immunoblotted for the indicated proteins on immunoprecipitated Flag-PABPC1. **(F)** Lentivirus-mediated PABPC1 transduction into endogenous *PABPC1*-inactivated H1703 cells induces PABPC1 expression at physiological levels of PABPC1 in lung cancer cells. **(G and H)** MKRN3 acts as a tumor suppressor by mediating the ubiquitination of PABPC1. H1703 cells were transduced with *PABPC1* sgRNA lentivirus to KO endogenous PABPC1. $H1703^{PABPC1\text{-}KO}$ cells were restored with WT or mutant PABPC1 and then restored with MKRN3. Cell viability (G) and anchorage-independent growth (H) in H1703 and H1437 cells were assessed by the cell viability assay and colony numbers, respectively (n = 3 per group; *, $P < 0.05$; **, $P < 0.01$; ***, $P < 0.001$; unpaired t test). All panels represent data from two or three independent experiments.

attributable to a single gene, *MKRN3*. There is increasing evidence that sex steroid hormones exert effects in nonreproductive organs, such as the lungs (Ben Khedher et al., 2017; Kreuzer et al., 2003). Sex steroid hormones and reproductive factors also play a role in the genesis of lung cancer (Ben Khedher et al., 2017; Kreuzer et al., 2003). Nonetheless, our findings provide a potential molecular mechanism. This mysterious and hidden connection may prove a boon in disguise and has raised hopes that studying the biology of one disease may help to identify novel therapeutic targets for the other.

Germline *MKRN3* mutations also cause Prader–Willi syndrome in humans. Reports of spontaneous lung cancer in patients with Prader–Willi syndrome suggest that germline *MKRN3* inactivation may predispose to lung cancer (Nenekidis et al., 2011) and suggest a possible link between genetic lesions present in Prader–Willi syndrome and enhanced/early-onset carcinogenesis in lung tumors. MKRN3 interacts with p53-regulated metabolic genes in a precocious puberty context (Yellapragada et al., 2019). Interestingly, genomic *MKRN3* aberrations occur frequently in human NSCLC samples harboring *TP53* mutations, suggesting that *TP53* and *MKRN3* mutations are not necessary in a mutually exclusive manner in the lung cancer context.

In summary, our genomic, functional, genetically engineered mouse model and mechanistic findings herein demonstrate that the tumor suppressor roles of MKRN3 contribute to NSCLC progression. MKRN3 dysregulation warrants evaluation as a potential point of therapeutic attack in KRAS-driven NSCLCs.

Materials and methods

Collection of human cancer datasets

We curated freely available somatic mutations from the data portal of TCGA (Cerami et al., 2012; Gao et al., 2013) and other published studies (Campbell et al., 2016; George et al., 2015; Govindan et al., 2012; Hellmann et al., 2018; Hoadley et al., 2018; Imielinski et al., 2012; Jamal-Hanjani et al., 2017; Peifer et al., 2012; Rudin et al., 2012; Shi et al., 2016).

Tumor and tissue samples

De-identified snap-frozen tumor biopsies and matched normal samples were from lung cancer patients at Shanghai Changzheng Hospital (approval no. 2019SL009). All samples were collected with institutional review board approval. Informed written consent was obtained from all human participants.

MKRN3 expression and patient survival analysis

To study the possible relationship between MKRN3 gene expression and survival, we first sorted patients from the TCGA and GEO datasets into MKRN3-high and MKRN3-low groups according to the MKRN3 mRNA relative expression levels (top 50% versus bottom 50%). Next, we analyzed the difference in survival between these two groups using GraphPad Prism 6.

Cell culture

HEK293T cells (American Type Culture Collection [ATCC]; catalog #ACS-4500) and the NSCLC cell lines NCI-H1703 (ATCC; catalog #CRL-5889) and NCI-H1437 (ATCC; catalog CRL-5872) were purchased from ATCC. HEK293T, NCI-H1703, and NCI-H1437 cells were maintained in RPMI 1640 (HyClone; #SH30027.01) medium containing 10% FBS (Thermo Fisher Scientific #10099141) and penicillin/streptomycin (Thermo Fisher Scientific; #15140122). All these cells were cultured at 37°C in a 5% CO_2 humidified atmosphere. None of the cell lines in this study appeared in the misidentified cell line list maintained by the International Cell Line Authentication Committee. All cell lines were routinely tested for microbial contamination (including mycoplasma).

Plasmid constructs and lentivirus production

The MKRN3 and PABPC1 expression plasmids were constructed by cloning the corresponding cDNAs into the p3×FLAG-CMV™-7.1 vector (Sigma-Aldrich; #E7533). PABPC1-ΔRRM1 (deleting aa 11–89), PABPC1-ΔRRM2 (deleting aa 99–175), PABPC1-ΔRRM3 (deleting aa 191–268), and PABPC1-ΔRRM4 (deleting aa 294–370) were generated by subcloning the corresponding cDNAs into the p3×FLAG-CMV™-7.1 vector. Hemagglutinin (HA)-Ub, HA-Ub-K48, and HA-Ub-K63 vectors were generously provided by Dr. Shao-Cong Sun (Department of Immunology, MD Anderson Cancer Center, The University of Texas, Houston, TX). PABPC1 K to R point mutants and MKRN3 point mutants were generated by introducing these mutations into the WT expression vector using the QuikChange Lightning Site-Directed Mutagenesis Kit (#210518). The PABPC1 single guide RNA (sgRNA; 5′-GCCCGG CGCTCACCGTCCGC-3′) vector was generated by cloning the PABPC1 targeting sgRNA into the lentiCRISPRv2 vector (Addgene; plasmid #52961). MKRN3 and PABPC1 lentiviral constructs were generated by cloning the corresponding cDNAs into the pCDH-CMV-MCS-EF1-Puro lentiviral expression vector (System Biosciences; catalog #CD510B-1). Lentivirus particles were generated by cotransfecting these lentiviral constructs and helper virus packaging plasmids pCMVΔR8.9 and pHCMV-VSV-G into

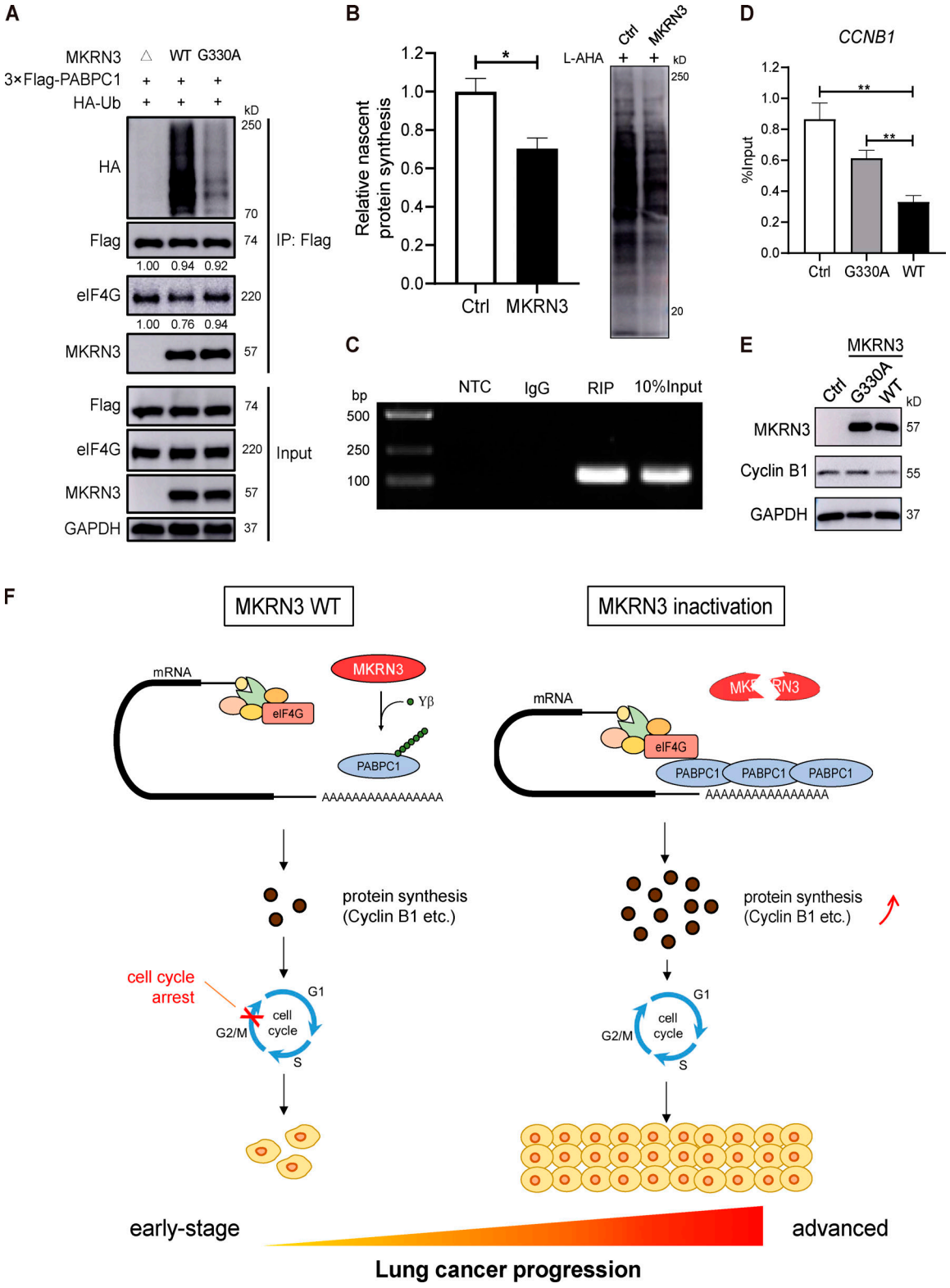

Figure 7. **MKRN3-PABPC1 axis regulates global protein translation in NSCLC. (A)** MKRN3 restoration compromises PABPC1-eIF4G interaction in the lung cancer cells. Coimmunoprecipitation assays were performed using anti-Flag antibody, followed by immunoblotting with indicated antibodies. Lung cancer–derived MKRN3 mutants, C258* (indicated by Δ) and G330A, serve as loss-of-functional controls. **(B)** MKRN3 restoration reduces global protein translation. Global translational activity detected by Click-it chemistry after labeling with L-AHA. Signal intensities of autoradiography analyses were quantified, and mean values from three independent experiments are represented. Representative lanes are shown on the right. Error bars indicate SEM (n = 3 per group; *, $P < 0.05$; unpaired t test). **(C)** PCR analysis of RIP demonstrating that PABPC1 binds to the 3′ poly(A) tail of *CCNB1* mRNA in the lung cancer context. RIP was performed using H1703 (Flag-PABPC1 transduced/endogenous *PABPC1*-inactivated; see Fig. 6 E) cell lysate and either anti-Flag or normal mouse IgG as the

immunoprecipitating antibody. Purified RNA was then analyzed by RT-PCR using RIP primers specific for the *CCNB1*. PCR product was observed in the anti-Flag RIP (lane 3) and was not detected in the IgG RIP (lane 2). *CCNB1* specific cDNA was also observed in the 10% input (lane 4) and not in the "No template" PCR control (NTC; lane 1). **(D)** MKRN3 restoration dramatically decreases the binding of PABPC1 to *CCNB1* mRNA in H1703 lung cancer cells. RIP assay was performed with the MKRN3 restored versus inactivated cells, and Flag-PABPC1–bound mRNAs were enriched with anti-Flag antibody followed by quantitative PCR assays. Data are presented as mean ± SD (n = 3 per group; **, P < 0.01; unpaired t test). **(E)** Western blotting showing that MKRN3 restoration reduces cyclin B1 expression. **(F)** A model depicting how the MKRN3-PABPC1 axis controls cell proliferation and progression in lung cancer. Left: The lung cancer cells with WT MKRN3. Right: The lung cancer cells with MKRN3 inactivation. The ubiquitination of PABPC1 by MKRN3 attenuates its binding to 3′ poly(A) tails of mRNAs and decreases the TIC formation. It thereby represses global protein synthesis and maintains lung cancer cells with limited proliferative capacity (left). Inactivated MKRN3 reduces PABPC1 ubiquitination, promotes its binding to 3′ poly(A) tails of mRNAs, and thereby accelerates global protein synthesis and promotes lung cancer proliferation and progression (right). All panels represent data from two or three independent experiments. Ctrl, control.

HEK293T cells using Lipofectamine 3000 (Invitrogen; #L3000015). Lentiviruses were harvested after 24, 36, 48, and 60 h and frozen at −80°C in aliquots at appropriate amounts for infection.

RT-PCR and quantitative PCR

Tissues were homogenized in TRIzol Reagent (Invitrogen; #15596026), followed by total RNA isolation using the standard protocol. RNA was further reverse-transcribed into cDNA using the HiScript III first Strand cDNA Synthesis Kit (+ genomic DNA wiper; Vazyme; #R312-01). PCR was performed for gene expression analysis of MKRN3 using 2×Taq Master Mix (Dye Plus; Vazyme; #P112-01); samples were run with non-RT or nontemplate control. Quantitative PCR was performed for target gene expression analysis using the ChamQ Universal SYBR qPCR Master Mix (Vazyme; #Q711-02). Samples were run in triplicate with non-RT or non–template control. Amplification accuracy was verified by melting curve analysis.

Soft agar assay and colony formation assay

6-well plates were first layered with 0.6% bottom agar (Noble agar; BD Difco; #214220) containing RPMI 1640 medium with 10% FBS and penicillin/streptomycin. H1703 (10,000 cells per well) and H1437 (10,000 cells per well) cells were transduced with control or MKRN3 lentivirus and seeded in 0.35% top agar containing 10% FBS and penicillin/streptomycin. Cells were allowed to grow for 4 wk and then stained with 1 ml of 1 mg/ml methyl thiazol tetrazolium (Sigma-Aldrich; #M5655) for 3 h. Colonies were counted by ImageJ software (National Institutes of Health). All assays were performed in triplicate wells, with the entire study replicated three times. A colony formation assay was conducted by seeding H1703 (500 cells per well) cells or H1437 (500 cells per well) cells transduced with the WT and truncating MKRN3 lentivirus into 6-well plates and allowed to grow for 3 wk. Then, the cells were fixed with 4% paraformaldehyde for 30 min and stained with crystal violet solution (Wuhan Servicebio Technology Co.; #G1014) for 3 h. All assays were performed in in triplicate wells, with the entire study replicated three times. Images were obtained using a scanner (Microtek; TMA 1600III).

Cell cycle and apoptosis assays

For cell cycle analysis, cells were grown until 70% confluence, serum-starved for 8 h (H1703) or 40 h (H1437) and washed with PBS. Cells were harvested and fixed in 70% ethanol for 24 h, resuspended in 50 μg/ml of propidium iodide (Sigma-Aldrich; #P4170) and 100 μg/ml of RNaseA (TIANGEN; #RT405) containing PBS solution after centrifugation, then were analyzed using the Gallios Flow Cytometer (Beckman Coulter) and ModFit LT software. For apoptosis analysis, cells were grown to 80% confluence, serum-starved for 3 d, then washed with PBS and harvested. Cells were stained with the APC Annexin V Apoptosis Detection Kit with 7-AAD (BioLegend; #640930) and evaluated by flow cytometry (Beckman Coulter; Gallios Flow Cytometer) according to the manufacturer's protocol.

Western blotting analysis

Whole-cell lysates from cell lines or frozen tissues were prepared using IP buffer (50 mM Tris-HCl, pH 8.0, 1% NP-40, 100 mM sodium fluoride, 2 mM sodium molybdate, 30 mM sodium pyrophosphate, 5 mM EDTA, and 2 mM sodium orthovanadate) containing protease inhibitors (10 μg/ml leupeptin, 10 μg/ml aprotinin, and 1 mM phenylmethylsulfonyl fluoride). The lysates were then rocked for 8 h (cell lines) or overnight (frozen tissues) at 4°C and cleared by centrifugation at 14,000 rpm for 30 min at 4°C. The protein concentrations in the lysate were determined using a Quick Start Bradford 1× Dye Reagent (Bio-Rad; #5000205). Electrophoresis and Western blotting were performed using standard techniques. The hybridization signals were detected by chemiluminescence (Immobilon Western, Millipore Corporation) and captured using an Amersham Imager 600 imagers (GE Healthcare; #29083461). The primary antibodies were list as follows: MKRN3 (Sigma-Aldrich, #HPA029494; Abcam, #ab177203), PABPC1 (ProteinTech; #10970-1-AP), Flag (Sigma-Aldrich; #F-1804), HA (ProteinTech; #51064-2-AP), Ub (Santa Cruz; #sc-8017), PCNA (Santa Cruz; #sc-56), β-actin (Sigma-Aldrich; #A4700), and GAPDH (Sigma-Aldrich; #G8795). Relative protein quantification was performed with Image Quant TL 8.1 (GE Healthcare) software. For cycloheximide chase assay, cells were treated with cycloheximide at 10 μM and harvested at the indicated time.

Immunohistochemistry

Immunohistochemistry was performed on tissue and tumor sections using MKRN3 (Sigma-Aldrich; #HPA029494), p40 (Maxim Biotech; #RMA-0815), or TTF1 (Maxim Biotech; #MAB-0599). Four-micron slides were deparaffinized in xylene and hydrated in a graded series of alcohol. Slides were then boiled by microwave for 12 min in citrate buffer (pH 6). Immunohistochemistry reactions were visualized by diaminobenzidine staining, using an EnVision+ system (Dako).

Mice

The animal experiments were approved by the Institutional Animal Care and Use Committee of the Shanghai Institutes for Biological Sciences, Chinese Academy of Science (approval no. SIBS-2017-WYX-1). All genetically engineered mice were from the C57BL/6 background. *MKRN3* straight KO (*Mkrn3*$^{p-/m+}$) mice were generated using the transcription activator-like effector nuclease–based approach to create a 2-bp deletion as previously described (Li et al., 2020; Fig. S4 B). *K-ras*$^{LSL-G12D/+}$ mice were purchased from The Jackson Laboratory (stock #008179). *Mkrn3*$^{pfl/m+}$ mice were generated as described in the conditional KO mouse model.

Xenograft tumor model

NCI-H1703 (2 × 10^6 cells) and NCI-H1437 (2 × 10^6 cells) cells transduced with MKRN3 WT and control lentivirus were injected subcutaneously into 6-wk-old male BALB/c nude mice, and tumor xenografts were allowed to grow for 4–5 wk. The resulting tumors were measured every 3 d. Tumor volume was calculated using the following formula: tumor volume = length × width × width/2. Once the largest tumor diameter reached the maximal tumor diameter allowed under our institutional protocol, all mice were killed, and tumors were collected. The maximal tumor diameter allowed by the Institutional Animal Care and Use Committee was 2.0 cm.

Urethane-induced mouse model

13 *MKRN3*$^{+/+}$ and 11 *MKRN3*$^{p-/m+}$ mice were given four intraperitoneal injections of urethane (Sigma-Aldrich; #U2500; 1 g/kg of body weight) weekly from 4 wk of age. Urethane was dissolved in 0.9% NaCl. Mice were euthanized by dislocation 12 mo after the last injection. Tumors were counted manually after dissection.

Conditional knock-out mouse model

Mice with a floxed *Mkrn3* exon 1 allele on the C57BL/6 background were generated as follows. We prepared a targeting construct including a 5.2-kb 5′ arm, a floxed fragment containing *Mkrn3* exon 1 and a neomycin positive selection cassette flanked by flippase recognition target sites, a 6.1-kb 3′ arm, and a thymidine kinase negative selection cassette. JM8A3 C57BL/6 embryonic stem cells were electroporated with the targeting vector and selected using G418 and ganciclovir. Three clones were identified with long-range PCR from 144 clones. The clonally expanded embryonic stem cells were injected into C57BL/6 blastocysts to generate chimeric mice. The *Mkrn3*$^{pfl/m+}$ mice were generated by crossing the chimeric mice with expressing Flp recombinase mice. KM mice were generated by crossing *MKRN3*$^{pfl/m+}$ male mice with *K-ras*$^{LSL-G12D/+}$ female mice. *K-ras*$^{LSL-G12D/+}$ mice, *Mkrn3*$^{pfl/m+}$ mice, and *K-ras*$^{LSL-G12D/+}$; *Mkrn3*$^{pfl/m+}$ mice were infected by intranasal instillation with adenovirus as previously described (DuPage et al., 2009). Mice were euthanized by dislocation 12 mo after intranasal instillation.

Mouse pathology

Lungs were perfused through the trachea with 4% paraformaldehyde, fixed overnight, transferred to 70% ethanol, and subsequently embedded in paraffin. Sections were cut at a thickness of 4 µm and stained with H&E for pathological examination. H&E-stained slides were scanned by an Aperio Imagescope (Leica).

IP and mass spectrometry

Cells were lysed by IP buffer containing protease inhibitors (10 µg/ml leupeptin, 10 µg/ml aprotinin, and 1 mM phenylmethylsulfonyl fluoride), mixed with 1 µg anti-Flag antibody and 20 µl protein G-sepharose (Thermo Fisher Scientific; #101242), incubated overnight, and eluted by boiling with SDS loading buffer. The eluted samples were detected by SDS-PAGE followed by Coomassie staining (Invitrogen; #LC6025; Colloidal Blue Staining Kit). For mass spectrometry, IP samples were eluted by shaking with 8 M urea and 100 mM Tris-Cl, pH 8.0, and analyzed by mass spectrometry.

Coimmunoprecipitation

Cells were lysed by IP buffer containing protease inhibitors (10 µg/ml leupeptin, 10 µg/ml aprotinin, and 1 mM phenylmethylsulfonyl fluoride), mixed with 2 µg anti-Flag antibody and 20 µl protein G-sepharose, and incubated overnight. Immunoprecipitates were eluted by boiling with SDS loading buffer. IP samples and whole-cell lysates were analyzed by Western blotting.

Ubiquitination assay

293T cells were transfected with MKRN3-WT or mutants, Flag-PABPC1-WT or mutants, and HA-Ub-WT or mutants, and then whole-cell lysates were immunoprecipitated with 2 µg anti-Flag antibody and analyzed by Western blotting with an anti-HA antibody. To analyze the ubiquitination of PABPC1 in H1703 cells, H1703 cells were infected with MKRN3 or control lentivirus, and then whole-cell lysates were immunoprecipitated with 4 µg anti-PABPC1 antibody and analyzed by Western blotting with an anti-Ub antibody.

Transcriptome sequencing

Total RNA was isolated from cells using standard Trizol protocol. Paired-end sequencing (2 × 100 bp) was performed with a BGI-500 instrument to obtain at least 20 million reads for each sample. The sequence data were processed and mapped to the human reference genome (hg19) using Bowtie2. Gene expression was quantified to fragments per kilobase per million mapped fragments using RNA sequencing by expectation maximization.

RNA IP (RIP) assay

RIP assay was performed using the EZ-Magna RIP Kit (Merck; #17-701). Cells were cultured in a 10-cm dish to 80–90% confluence. One RIP reaction required 100 µl of cell lysate from ∼2.0 × 10^7 cells. Cells were washed by PBS, collected by scraping, and suspended by RIP Lysis Buffer (Merck; #CS203176). Next, 5 µg of purified antibodies or corresponding IgG was added to the 100-µl cell lysate, and the mixture was incubated with rotation overnight at 4°C. Anti-Flag (Sigma-Aldrich; #F-1804) and normal mouse IgG (Merck; #CS200621) were used for RIP assay. The immunoprecipitated RNA was purified and analyzed with RT quantitative PCR.

Nascent protein measurement

300,000 cells were seeded and transduced with MKRN3 and control lentivirus. 60 h later, the medium was replaced with methionine-free medium (Thermo Fisher Scientific; #A1451701) for 2 h. Cells were incubated with 50 µM L-AHA (Clickchemistrytools; #1066-25) for 8 h and harvested in lysis buffer. L-AHA was detected using click chemistry with 50 µM Biotin Alkyne (Clickchemistrytools; #1266–5) with the Click-&-Go Protein Reaction Buffer Kit (Clickchemistrytools; #1262) per the manufacturer's protocol. The extracted protein was detected by Western blotting as described above. The blots were probed with a horseradish peroxidase–conjugated streptavidin (Proteintech; #SA0001) and developed with Enhanced Chemiluminescence (GE; #RPN2232).

Co-occurrence/mutual exclusivity

The DISCOVER method was used to determine significant mutual exclusivity and cooccurrence between *MKRN3* and *KRAS* mutations in the five NSCLC cohorts as previously described (Canisius et al., 2016).

Statistical analysis

Statistical analysis was performed using GraphPad Prism 6 (GraphPad Software). The difference between two groups was analyzed by paired sample *t* test. The differences among multiple groups were analyzed by one-way ANOVA.

Online supplemental material

Fig. S1 presents the genomic *MKRN3* aberrations in human NSCLCs. Fig. S2 shows effects of 5-aza-2′-deoxycytidine on MKRN3 expression in NSCLC cell lines and cell apoptosis caused by MKRN3 restoration in MKRN3-inactivated lung cancer cells. Fig. S3 demonstrates that MKRN3 restoration in *MKRN3*-inactivated H1703 lung cancer cells reduces cell proliferation. Fig. S4 displays MKRN3 inactivation in *Mkrn3* straight KO ($Mkrn3^{p-/m+}$) mice and *Mkrn3* conditional KO ($Mkrn3^{pfl/m+}$) mice. Fig. S5 shows that MKRN3 mediates PABPC1 ubiquitination. Table S1 shows clinicopathologic classification for 67 NSCLCs with genomic MKRN3 aberrations from TCGA lung cancer datasets. Table S2 shows clinicopathologic classification and MKRN3 protein expression in 30 NSCLCs from Asian patients. Table S3 shows gene expression profiling by RNA sequencing 96 hours after MKRN3 restoration in MKRN3-deficient/MKRN3-mutant H1703 cells. Table S4 shows primers used in the study.

Data availability

RNA sequencing datasets for MKRN3-deficient/MKRN3 mutant H1703 cells are available in the National Omics Data Encyclopedia (https://www.biosino.org/node/) under accession no. OEP002179.

Acknowledgments

We thank Drs. Ronggui Hu and Chuanyin Li (State Key Laboratory of Molecular Biology, Shanghai Institute of Biochemistry and Cell Biology, Center for Excellence in Molecular Cell Science, Chinese Academy of Sciences, Shanghai, China) for providing *MKRN3* straight KO mice and sharing PABPC1 as a substrate of MKRN3 in the precocious puberty context. We also thank Dr. Jun Qin (Shanghai Institute of Nutrition and Health, Chinese Academy of Sciences, Shanghai, China) for Kaplan–Meier survival analysis and all members of the Wang laboratory for thought-provoking discussion, technical assistance, and help with manuscript preparation.

This work was supported by grants from the National Natural Science Foundation of China (82072974, 81572642), the Basic Research Project of Shanghai Science and Technology Commission (20JC1419200), the National Key Research and Development Program of China (2016YFC1302100), the China Medicine Education Association (2021-002), the Key Laboratory of Tissue Microenvironment and Tumor of the Chinese Academy of Sciences (202002), the Chinese Academy of Sciences, and Shanghai Changzheng Hospital.

Author contributions: Y. Wang and K. Li conceived and designed the research. K. Li, X. Zheng, H. Tang, Y.-S. Zang, C. Zeng, X. Liu, Y. Shen, Y. Pang, S. Wang, F. Xie, X. Lu, Y. Luo, Z. Li, W. Bi, X. Jia, T. Huang, Q. Zhu, X. Zhang, and Y. Wang performed experiments. H. Tang, R. Wei, K. Huang, and Z. Chen provided samples and clinical data. K. Li, X. Zheng, H. Tang, Y.-S. Zang, C. Zeng, X. Liu, Y. Shen, Y. Pang, S. Wang, F. Xie, X. Lu, Y. Luo, Z. Li, W. Bi, X. Jia, T. Huang, Q. Zhu, Y. He, M. Zhang, Z. Gu, Y. Xiao, X. Zhang, and Y. Wang analyzed data. Y. Zhang, M. Zhang, Z. Gu, Y. Xiao, X. Zhang, and J.A. Fletcher provided scientific advice and helpful comments on the project. K. Li, X. Zheng, and Y. Wang wrote the manuscript. All authors read and approved the final manuscript.

Disclosures: The authors declare no competing interests exist.

Submitted: 19 January 2021
Revised: 23 April 2021
Accepted: 25 May 2021

References

Abreu, A.P., A. Dauber, D.B. Macedo, S.D. Noel, V.N. Brito, J.C. Gill, P. Cukier, I.R. Thompson, V.M. Navarro, P.C. Gagliardi, et al. 2013. Central precocious puberty caused by mutations in the imprinted gene MKRN3. *N. Engl. J. Med.* 368:2467–2475. https://doi.org/10.1056/NEJMoa1302160

Abreu, A.P., C.A. Toro, Y.B. Song, V.M. Navarro, M.A. Bosch, A. Eren, J.N. Liang, R.S. Carroll, A.C. Latronico, O.K. Rønnekleiv, et al. 2020. MKRN3 inhibits the reproductive axis through actions in kisspeptin-expressing neurons. *J. Clin. Invest.* 130:4486–4500.

Adzhubei, I.A., S. Schmidt, L. Peshkin, V.E. Ramensky, A. Gerasimova, P. Bork, A.S. Kondrashov, and S.R. Sunyaev. 2010. A method and server for predicting damaging missense mutations. *Nat. Methods.* 7:248–249. https://doi.org/10.1038/nmeth0410-248

Ben Khedher, S., M. Neri, A. Papadopoulos, D.C. Christiani, N. Diao, C.C. Harris, S. Olivo-Marston, A.G. Schwartz, M. Cote, A. Koushik, et al. 2017. Menstrual and reproductive factors and lung cancer risk: A pooled analysis from the international lung cancer consortium. *Int. J. Cancer.* 141:309–323. https://doi.org/10.1002/ijc.30750

Bretones, G., M.G. Álvarez, J.R. Arango, D. Rodríguez, F. Nadeu, M.A. Prado, R. Valdés-Mas, D.A. Puente, J.A. Paulo, J. Delgado, et al. 2018. Altered patterns of global protein synthesis and translational fidelity in RPS15-mutated chronic lymphocytic leukemia. *Blood.* 132:2375–2388. https://doi.org/10.1182/blood-2017-09-804401

Calcaterra, V., G. Nakib, G. Pelizzo, B. Rundo, G. Anna Rispoli, S. Boghen, F. Bonetti, B. Del Monte, C. Gertosio, and D. Larizza. 2013. Central precocious puberty and granulosa cell ovarian tumor in an 8-year old female. *Pediatr. Rep.* 5:e13. https://doi.org/10.4081/pr.2013.e13

Campbell, J.D., A. Alexandrov, J. Kim, J. Wala, A.H. Berger, C.S. Pedamallu, S.A. Shukla, G. Guo, A.N. Brooks, B.A. Murray, et al. Cancer Genome Atlas Research Network. 2016. Distinct patterns of somatic genome alterations in lung adenocarcinomas and squamous cell carcinomas. *Nat. Genet.* 48:607–616. https://doi.org/10.1038/ng.3564

Canisius, S., J.W.M. Martens, and L.F.A. Wessels. 2016. A novel independence test for somatic alterations in cancer shows that biology drives mutual exclusivity but chance explains most co-occurrence. *Genome Biol.* 17:261. https://doi.org/10.1186/s13059-016-1114-x

Cerami, E., J. Gao, U. Dogrusoz, B.E. Gross, S.O. Sumer, B.A. Aksoy, A. Jacobsen, C.J. Byrne, M.L. Heuer, E. Larsson, et al. 2012. The cBio cancer genomics portal: an open platform for exploring multidimensional cancer genomics data. *Cancer Discov.* 2:401–404. https://doi.org/10.1158/2159-8290.CD-12-0095

Day, F.R., D.J. Thompson, H. Helgason, D.I. Chasman, H. Finucane, P. Sulem, K.S. Ruth, S. Whalen, A.K. Sarkar, E. Albrecht, et al. PRACTICAL consortium. 2017. Genomic analyses identify hundreds of variants associated with age at menarche and support a role for puberty timing in cancer risk. *Nat. Genet.* 49:834–841. https://doi.org/10.1038/ng.3841

DuPage, M., A.L. Dooley, and T. Jacks. 2009. Conditional mouse lung cancer models using adenoviral or lentiviral delivery of Cre recombinase. *Nat. Protoc.* 4:1064–1072. https://doi.org/10.1038/nprot.2009.95

Ebright, R.Y., S. Lee, B.S. Wittner, K.L. Niederhoffer, B.T. Nicholson, A. Bardia, S. Truesdell, D.F. Wiley, B. Wesley, S. Li, et al. 2020. Deregulation of ribosomal protein expression and translation promotes breast cancer metastasis. *Science.* 367:1468–1473. https://doi.org/10.1126/science.aay0939

Fang, Y., H. Yu, X. Liang, J. Xu, and X. Cai. 2014. Chk1-induced CCNB1 overexpression promotes cell proliferation and tumor growth in human colorectal cancer. *Cancer Biol. Ther.* 15:1268–1279. https://doi.org/10.4161/cbt.29691

Gao, J., B.A. Aksoy, U. Dogrusoz, G. Dresdner, B. Gross, S.O. Sumer, Y. Sun, A. Jacobsen, R. Sinha, E. Larsson, et al. 2013. Integrative analysis of complex cancer genomics and clinical profiles using the cBioPortal. *Sci. Signal.* 6:pl1. https://doi.org/10.1126/scisignal.2004088

George, J., J.S. Lim, S.J. Jang, Y. Cun, L. Ozretić, G. Kong, F. Leenders, X. Lu, L. Fernández-Cuesta, G. Bosco, et al. 2015. Comprehensive genomic profiles of small cell lung cancer. *Nature.* 524:47–53. https://doi.org/10.1038/nature14664

Ghandi, M., F.W. Huang, J. Jané-Valbuena, G.V. Kryukov, C.C. Lo, E.R. McDonald III, J. Barretina, E.T. Gelfand, C.M. Bielski, H. Li, et al. 2019. Next-generation characterization of the Cancer Cell Line Encyclopedia. *Nature.* 569:503–508. https://doi.org/10.1038/s41586-019-1186-3

Govindan, R., L. Ding, M. Griffith, J. Subramanian, N.D. Dees, K.L. Kanchi, C.A. Maher, R. Fulton, L. Fulton, J. Wallis, et al. 2012. Genomic landscape of non-small cell lung cancer in smokers and never-smokers. *Cell.* 150:1121–1134. https://doi.org/10.1016/j.cell.2012.08.024

Hellmann, M.D., T. Nathanson, H. Rizvi, B.C. Creelan, F. Sanchez-Vega, A. Ahuja, A. Ni, J.B. Novik, L.M.B. Mangarin, M. Abu-Akeel, et al. 2018. Genomic features of response to combination immunotherapy in patients with advanced non-small-cell lung cancer. *Cancer Cell.* 33:843–852.e4. https://doi.org/10.1016/j.ccell.2018.03.018

Hellmann, M.D., L. Paz-Ares, R. Bernabe Caro, B. Zurawski, S.W. Kim, E. Carcereny Costa, K. Park, A. Alexandru, L. Lupinacci, E. de la Mora Jimenez, et al. 2019. Nivolumab plus Ipilimumab in Advanced Non-Small-Cell Lung Cancer. *N. Engl. J. Med.* 381:2020–2031. https://doi.org/10.1056/NEJMoa1910231

Hoadley, K.A., C. Yau, T. Hinoue, D.M. Wolf, A.J. Lazar, E. Drill, R. Shen, A.M. Taylor, A.D. Cherniack, V. Thorsson, et al. Cancer Genome Atlas Network. 2018. Cell-of-origin patterns dominate the molecular classification of 10,000 tumors from 33 types of cancer. *Cell.* 173:291–304.e6. https://doi.org/10.1016/j.cell.2018.03.022

Hoffman, E.P., R.H. Brown Jr., and L.M. Kunkel. 1987. Dystrophin: the protein product of the Duchenne muscular dystrophy locus. *Cell.* 51:919–928. https://doi.org/10.1016/0092-8674(87)90579-4

Holmes, D. 2017. Reproductive endocrinology: Puberty timing and cancer risk. *Nat. Rev. Endocrinol.* 13:377. https://doi.org/10.1038/nrendo.2017.63

Hong, D.S., M.G. Fakih, J.H. Strickler, J. Desai, G.A. Durm, G.I. Shapiro, G.S. Falchook, T.J. Price, A. Sacher, C.S. Denlinger, et al. 2020. KRAS^{G12C} Inhibition with Sotorasib in Advanced Solid Tumors. *N. Engl. J. Med.* 383:1207–1217. https://doi.org/10.1056/NEJMoa1917239

Hyer, M.L., M.A. Milhollen, J. Ciavarri, P. Fleming, T. Traore, D. Sappal, J. Huck, J. Shi, J. Gavin, J. Brownell, et al. 2018. A small-molecule inhibitor of the ubiquitin activating enzyme for cancer treatment. *Nat. Med.* 24:186–193. https://doi.org/10.1038/nm.4474

Imielinski, M., A.H. Berger, P.S. Hammerman, B. Hernandez, T.J. Pugh, E. Hodis, J. Cho, J. Suh, M. Capelletti, A. Sivachenko, et al. 2012. Mapping the hallmarks of lung adenocarcinoma with massively parallel sequencing. *Cell.* 150:1107–1120. https://doi.org/10.1016/j.cell.2012.08.029

Ishida, S., F. Picard, G. Rudolf, E. Noé, G. Achaz, P. Thomas, P. Genton, E. Mundwiller, M. Wolff, C. Marescaux, et al. 2013. Mutations of DEPDC5 cause autosomal dominant focal epilepsies. *Nat. Genet.* 45:552–555. https://doi.org/10.1038/ng.2601

Jackson, E.L., K.P. Olive, D.A. Tuveson, R. Bronson, D. Crowley, M. Brown, and T. Jacks. 2005. The differential effects of mutant p53 alleles on advanced murine lung cancer. *Cancer Res.* 65(22):10280–10288. https://doi.org/10.1158/0008-5472.CAN-05-2193

Jamal-Hanjani, M., G.A. Wilson, N. McGranahan, N.J. Birkbak, T.B.K. Watkins, S. Veeriah, S. Shafi, D.H. Johnson, R. Mitter, R. Rosenthal, et al. TRACERx Consortium. 2017. Tracking the evolution of non-small-cell lung cancer. *N. Engl. J. Med.* 376:2109–2121. https://doi.org/10.1056/NEJMoa1616288

Kim, Y., H.M. Lee, Y. Xiong, N. Sciaky, S.W. Hulbert, X. Cao, J.I. Everitt, J. Jin, B.L. Roth, and Y.H. Jiang. 2017. Targeting the histone methyltransferase G9a activates imprinted genes and improves survival of a mouse model of Prader-Willi syndrome. *Nat. Med.* 23:213–222. https://doi.org/10.1038/nm.4257

Komander, D., and M. Rape. 2012. The ubiquitin code. *Annu. Rev. Biochem.* 81:203–229. https://doi.org/10.1146/annurev-biochem-060310-170328

Kreuzer, M., M. Gerken, J. Heinrich, L. Kreienbrock, and H.E. Wichmann. 2003. Hormonal factors and risk of lung cancer among women? *Int. J. Epidemiol.* 32:263–271. https://doi.org/10.1093/ije/dyg064

Kwon, Y.T., and A. Ciechanover. 2017. The ubiquitin code in the ubiquitin-proteasome system and autophagy. *Trends Biochem. Sci.* 42:873–886. https://doi.org/10.1016/j.tibs.2017.09.002

Latronico, A.C., V.N. Brito, and J.C. Carel. 2016. Causes, diagnosis, and treatment of central precocious puberty. *Lancet Diabetes Endocrinol.* 4:265–274. https://doi.org/10.1016/S2213-8587(15)00380-0

Li, C., W. Lu, L. Yang, Z. Li, X. Zhou, R. Guo, J. Wang, Z. Wu, Z. Dong, G. Ning, et al. 2020. MKRN3 regulates the epigenetic switch of mammalian puberty via ubiquitination of MBD3. *Natl. Sci. Rev.* 7:671–685. https://doi.org/10.1093/nsr/nwaa023

Li, C., T. Han, Q. Li, M. Zhang, R. Guo, Y. Yang, W. Lu, Z. Li, C. Peng, P. Wu, et al. 2021. MKRN3-mediated ubiquitination of Poly(A)-binding proteins modulates the stability and translation of GNRH1 mRNA in mammalian puberty. *Nucleic Acids Res.* 49:3796–3813. https://doi.org/10.1093/nar/gkab155

Lindqvist, L.M., K. Tandoc, I. Topisirovic, and L. Furic. 2018. Cross-talk between protein synthesis, energy metabolism and autophagy in cancer. *Curr. Opin. Genet. Dev.* 48:104–111. https://doi.org/10.1016/j.gde.2017.11.003

Mainardi, S., A. Mulero-Sánchez, A. Prahallad, G. Germano, A. Bosma, P. Krimpenfort, C. Lieftink, J.D. Steinberg, N. de Wit, S. Gonçalves-Ribeiro, et al. 2018. SHP2 is required for growth of KRAS-mutant non-small-cell lung cancer in vivo. *Nat. Med.* 24:961–967. https://doi.org/10.1038/s41591-018-0023-9

McLoed, A.G., T.P. Sherrill, D.S. Cheng, W. Han, J.A. Saxon, L.A. Gleaves, P. Wu, V.V. Polosukhin, M. Karin, F.E. Yull, et al. 2016. Neutrophil-Derived IL-1β Impairs the Efficacy of NF-κB Inhibitors against Lung Cancer. *Cell Rep.* 16:120–132. https://doi.org/10.1016/j.celrep.2016.05.085

Nenekidis, I., G.T. Stathopoulos, V. Anagnostakou, A. Kokkori, P. Dedeilias, J. Kokotsakis, M. Argiriou, and C. Zisis. 2011. Atypical pulmonary carcinoid tumour in a 28-year-old nonsmoker with Prader-Willi syndrome. *Eur. Respir. J.* 38:1230–1233. https://doi.org/10.1183/09031936.00034711

Nguyen, H.G., C.S. Conn, Y. Kye, L. Xue, C.M. Forester, J.E. Cowan, A.C. Hsieh, J.T. Cunningham, C. Truillet, F. Tameire, et al. 2018. Development of a stress response therapy targeting aggressive prostate cancer. *Sci. Transl. Med.* 10:eaar2036. https://doi.org/10.1126/scitranslmed.aar2036

Pang, Y., F. Xie, H. Cao, C. Wang, M. Zhu, X. Liu, X. Lu, T. Huang, Y. Shen, K. Li, et al. 2019. Mutational inactivation of mTORC1 repressor gene *DEPDC5* in human gastrointestinal stromal tumors. *Proc. Natl. Acad. Sci. USA.* 116:22746–22753. https://doi.org/10.1073/pnas.1914542116

Pao, W., and J. Chmielecki. 2010. Rational, biologically based treatment of EGFR-mutant non-small-cell lung cancer. *Nat. Rev. Cancer.* 10:760–774. https://doi.org/10.1038/nrc2947

Peifer, M., L. Fernández-Cuesta, M.L. Sos, J. George, D. Seidel, L.H. Kasper, D. Plenker, F. Leenders, R. Sun, T. Zander, et al. 2012. Integrative genome analyses identify key somatic driver mutations of small-cell lung cancer. *Nat. Genet.* 44:1104–1110. https://doi.org/10.1038/ng.2396

Pelletier, J., G. Thomas, and S. Volarević. 2018. Ribosome biogenesis in cancer: new players and therapeutic avenues. *Nat. Rev. Cancer.* 18:51–63. https://doi.org/10.1038/nrc.2017.104

Popovic, D., D. Vucic, and I. Dikic. 2014. Ubiquitination in disease pathogenesis and treatment. *Nat. Med.* 20:1242–1253. https://doi.org/10.1038/nm.3739

Rex, T.S., K. Boyd, T. Apple, C. Bricker-Anthony, K. Vail, and J. Wallace. 2016. Effects of repeated anesthesia containing urethane on tumor formation and health scores in male C57BL/6J mice. *J. Am. Assoc. Lab. Anim. Sci.* 55: 295–299.

Rudin, C.M., S. Durinck, E.W. Stawiski, J.T. Poirier, Z. Modrusan, D.S. Shames, E.A. Bergbower, Y. Guan, J. Shin, J. Guillory, et al. 2012. Comprehensive genomic analysis identifies SOX2 as a frequently amplified gene in small-cell lung cancer. *Nat. Genet.* 44:1111–1116. https://doi.org/10.1038/ng.2405

Senft, D., J. Qi, and Z.A. Ronai. 2018. Ubiquitin ligases in oncogenic transformation and cancer therapy. *Nat. Rev. Cancer.* 18:69–88. https://doi.org/10.1038/nrc.2017.105

Shaw, A.T., and J.A. Engelman. 2013. ALK in lung cancer: past, present, and future. *J. Clin. Oncol.* 31:1105–1111. https://doi.org/10.1200/JCO.2012.44.5353

Shi, J., X. Hua, B. Zhu, S. Ravichandran, M. Wang, C. Nguyen, S.A. Brodie, A. Palleschi, M. Alloisio, G. Pariscenti, et al. 2016. Somatic genomics and clinical features of lung adenocarcinoma: a retrospective study. *PLoS Med.* 13:e1002162. https://doi.org/10.1371/journal.pmed.1002162

Shin, Y.L. 2016. An update on the genetic causes of central precocious puberty. *Ann. Pediatr. Endocrinol. Metab.* 21:66–69. https://doi.org/10.6065/apem.2016.21.2.66

Siegel, R.L., K.D. Miller, and A. Jemal. 2020. Cancer statistics, 2020. *CA Cancer J. Clin.* 70:7–30. https://doi.org/10.3322/caac.21590

Teixeira, V.H., C.P. Pipinikas, A. Pennycuick, H. Lee-Six, D. Chandrasekharan, J. Beane, T.J. Morris, A. Karpathakis, A. Feber, C.E. Breeze, et al. 2019. Deciphering the genomic, epigenomic, and transcriptomic landscapes of pre-invasive lung cancer lesions. *Nat. Med.* 25:517–525. https://doi.org/10.1038/s41591-018-0323-0

To, M.D., C.E. Wong, A.N. Karnezis, R. Del Rosario, R. Di Lauro, and A. Balmain. 2008. Kras regulatory elements and exon 4A determine mutation specificity in lung cancer. *Nat. Genet.* 40:1240–1244. https://doi.org/10.1038/ng.211

Tritschler, F., E. Huntzinger, and E. Izaurralde. 2010. Role of GW182 proteins and PABPC1 in the miRNA pathway: a sense of déjà vu. *Nat. Rev. Mol. Cell Biol.* 11:379–384. https://doi.org/10.1038/nrm2885

Wang, Y., A. Marino-Enriquez, R.R. Bennett, M. Zhu, Y. Shen, G. Eilers, J.C. Lee, J. Henze, B.S. Fletcher, Z. Gu, et al. 2014. Dystrophin is a tumor suppressor in human cancers with myogenic programs. *Nat. Genet.* 46: 601–606. https://doi.org/10.1038/ng.2974

Xie, J., G. Kozlov, and K. Gehring. 2014. The "tale" of poly(A) binding protein: the MLLE domain and PAM2-containing proteins. *Biochim. Biophys. Acta.* 1839:1062–1068. https://doi.org/10.1016/j.bbagrm.2014.08.001

Xie, X., H. Hu, X. Tong, L. Li, X. Liu, M. Chen, H. Yuan, X. Xie, Q. Li, Y. Zhang, et al. 2018. The mTOR-S6K pathway links growth signalling to DNA damage response by targeting RNF168. *Nat. Cell Biol.* 20:320–331. https://doi.org/10.1038/s41556-017-0033-8

Yatabe, Y., S. Dacic, A.C. Borczuk, A. Warth, P.A. Russell, S. Lantuejoul, M.B. Beasley, E. Thunnissen, G. Pelosi, N. Rekhtman, et al. 2019. Best practices recommendations for diagnostic immunohistochemistry in lung cancer. *J. Thorac. Oncol.* 14:377–407. https://doi.org/10.1016/j.jtho.2018.12.005

Yellapragada, V., X. Liu, C. Lund, J. Känsäkoski, K. Pulli, S. Vuoristo, K. Lundin, T. Tuuri, M. Varjosalo, and T. Raivio. 2019. MKRN3 Interacts With Several Proteins Implicated in Puberty Timing but Does Not Influence *GNRH1* Expression. *Front. Endocrinol. (Lausanne).* 10:48. https://doi.org/10.3389/fendo.2019.00048

Supplemental material

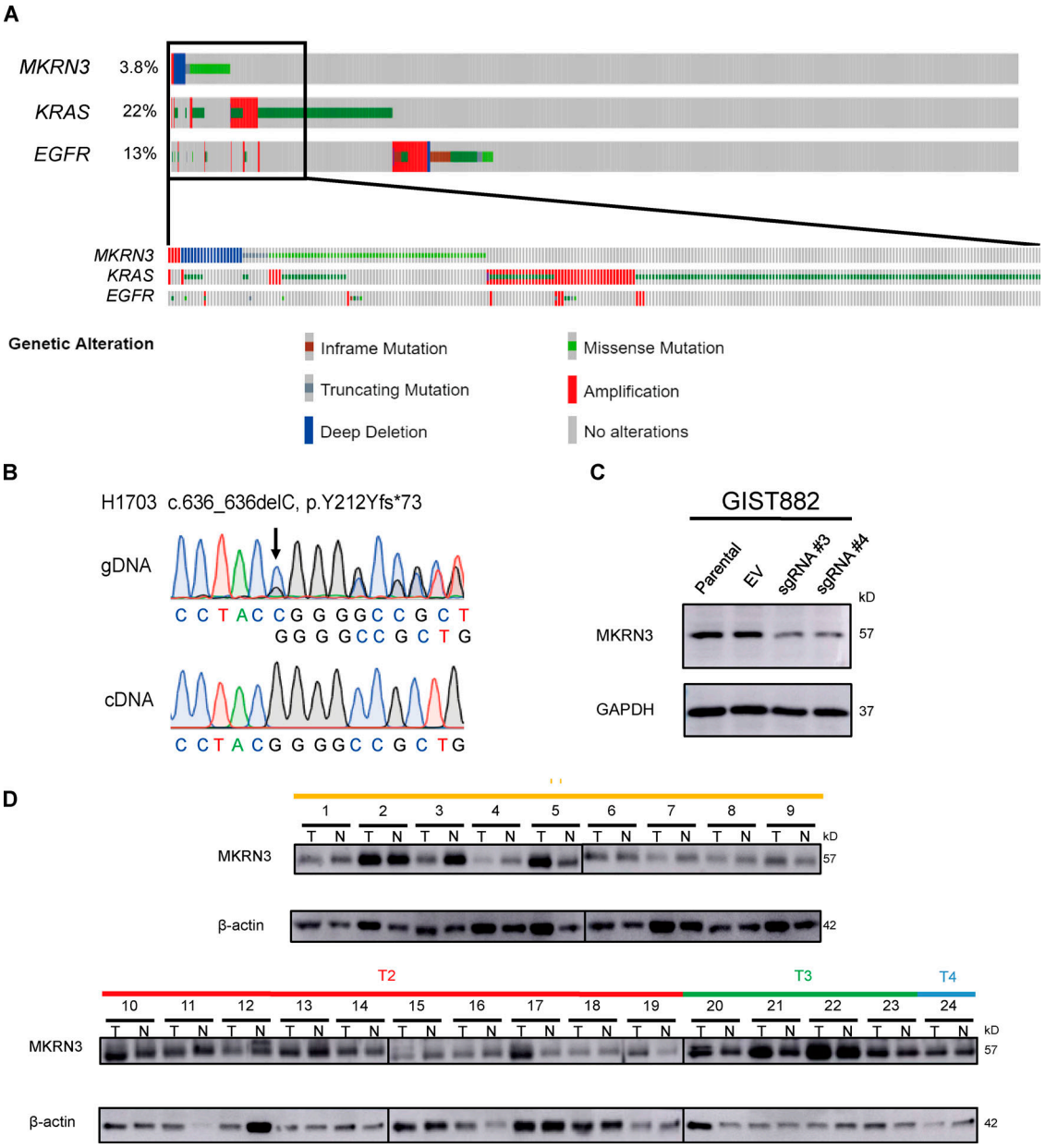

Figure S1. **Genomic *MKRN3* aberrations in human NSCLCs. (A)** OncoPrint plot showing *MKRN3*, *KRAS*, and *EGFR* genomic alterations across 1,758 NSCLC samples. Percentages on the left indicate samples with the displayed alterations. Analysis performed using sequencing and copy number alterations data from TCGA in cBioPortal. **(B)** Sequence tracings of genomic DNA and cDNA from H1703 cells derived from NSCLC patients with a heterozygous *MKRN3* mutation. Both alleles are detectable in genomic DNA (gDNA), but only the mutant allele is present in cDNA, indicating that only the mutant *MKRN3* allele is transcribed. **(C)** Validation of MKRN3 antibody (Abcam; #ab177203) to detect endogenous MRKN3 protein by Western blotting analysis. CRISPR-mediated MKRN3 knockdown in a gastrointestinal stromal tumor (GIST) cell line (GIST882) results in MKRN3 down-regulation. EV, empty vector. **(D)** Decreased MKRN3 protein expression in the NSCLC lysates as compared with the adjacent normal counterparts. MKRN3 protein levels in 24 pairs of NSCLC samples. T, lung tumor tissues; N, matched adjacent normal tissues. All panels represent data from two independent experiments.

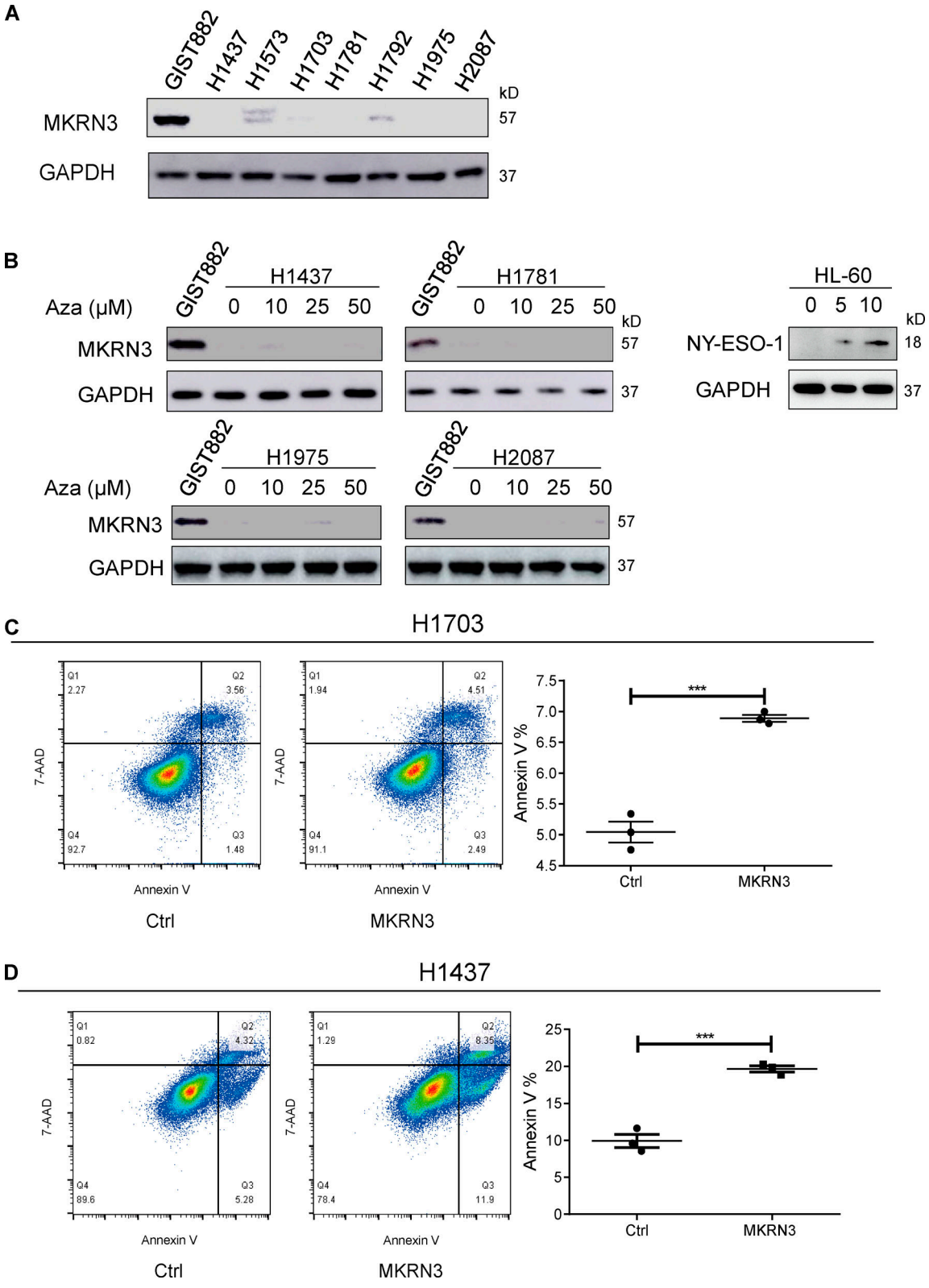

Figure S2. **Effects of 5-aza-2′-deoxycytidine on MKRN3 expression in NSCLC cell lines and cell apoptosis caused by MKRN3 restoration in MKRN3-inactivated lung cancer cells. (A)** MKRN3 expression in NSCLC cell lines. Gastrointestinal stromal tumor cell line (GIST882) is positive control. **(B)** HL-60 (human promyelocytic leukemia cell line) and NSCLC cell lines were treated with 5-aza-2′-deoxycytidine (Aza, a DNA methyltransferase inhibitor) at indicated concentrations. Aza treatment restored NY-ESO-1 expression in HL-60 cells but could not restore MKRN3 expression in NSCLC cell lines with MKRN3 inactivation. **(C and D)** MKRN3 restoration in MKRN3-inactivated H1703 and H1437 lung cancer cells increases cell apoptosis. Flow cytometry analyses demonstrating increased apoptosis levels in MKRN3-restored H1703 (C) and H1437 (D) cells. Experiments were performed in triplicate (***, $P < 0.001$; unpaired *t* test). All panels represent data from two independent experiments. Ctrl, control.

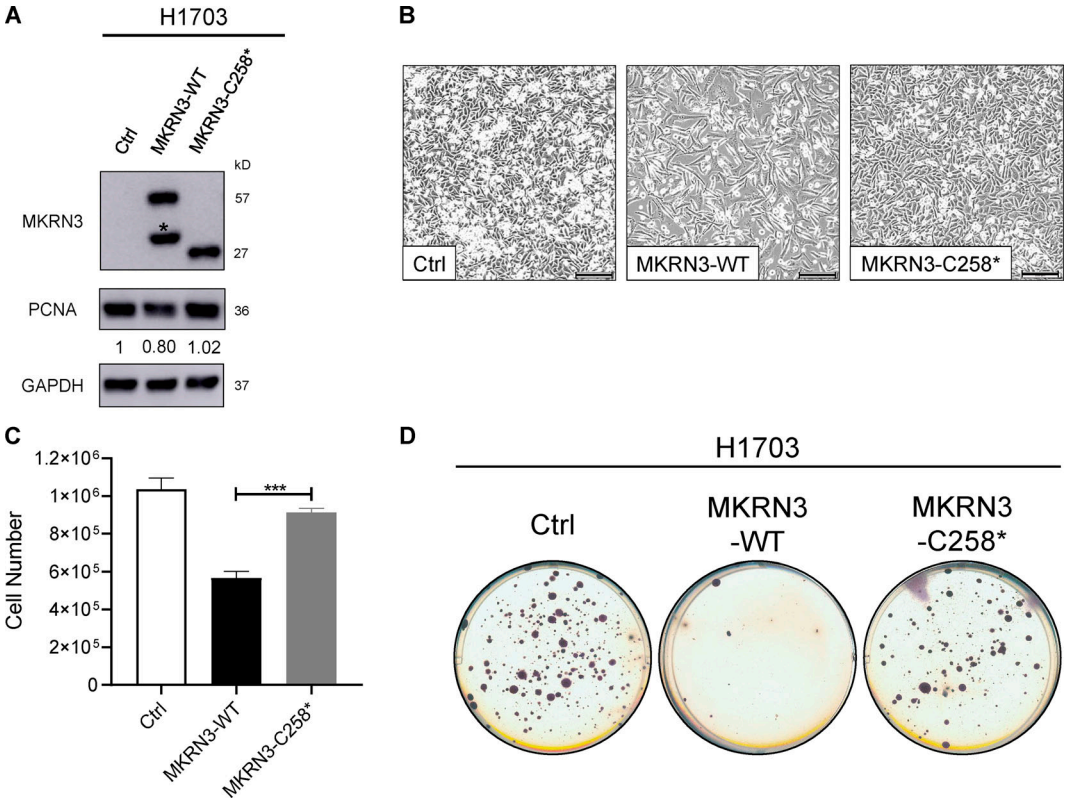

Figure S3. **MKRN3 restoration in *MKRN3*-inactivated H1703 lung cancer cells reduces cell proliferation. (A)** MKRN3 reexpression induces expression of WT MKRN3 (57 kD) at levels comparable to those of C258* truncation mutant (27 kD) restoration. Asterisk indicates nonspecific band. **(B and C)** Lentivirus-mediated MKRN3 restoration reduces the viability of H1703 cells, as assessed by representative bright field microscopy images (B) and cell counting (C). Scale bar, 200 µm. ***, $P < 0.001$; unpaired *t* test. **(D)** MKRN3 restoration suppresses anchorage-independent growth of H1703 cells. Experiments were performed in triplicate. All panels represent data from three independent experiments.

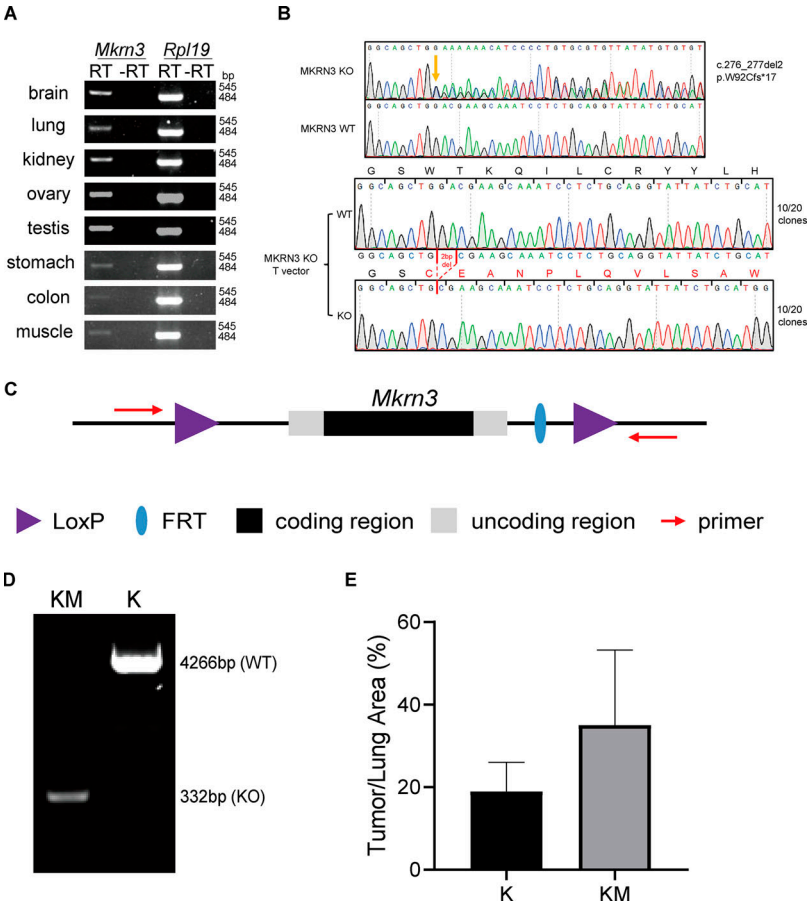

Figure S4. **MKRN3 inactivation in *Mkrn3* straight KO (*Mkrn3*$^{p-/m+}$) mice and *Mkrn3* conditional KO (*Mkrn3*$^{pfl/m+}$) mice. (A)** RT-PCR demonstrates MKRN3 expression in a variety of mouse tissues, including brain, lung, kidney, stomach, colon, muscle, ovary, and testis. RPL19 was included as a loading control. -RT indicates samples treated without RT. MKRN3 is an intronless gene. Therefore, a DNase treatment was performed on the RNA samples to digest the genomic DNA. **(B)** *Mkrn3* straight KO (*Mkrn3*$^{p-/m+}$) mice show frameshift deletion (2-bp deletion) in *MKRN3*. Sanger sequencing confirms heterozygous frameshift mutation (c.276_277delGA; p.W92Cfs*17) of *MKRN3* in *Mkrn3*$^{p-/m+}$ mice as previously described (Li et al., 2020). p, paternally inherited allele; m, maternally inherited allele; +, WT; -, KO. By subcloning and sequencing 20 independent clones from the Sanger PCR fragment, 10 out of 20 clones harbor the frameshift mutation, introducing a premature stop codon 17 amino acids downstream. The yellow arrow indicates the start of the deletion site. **(C and D)** *Mkrn3* conditional KO (*Mkrn3*$^{pfl/m+}$) mice show *Mkrn3* deletion. **(C)** Schematic diagram of floxed cassette across *Mkrn3* locus. FRT, flippase recognition target. **(D)** Detection of *Mkrn3* deleted locus in the lung of KM mice by PCR. Template DNA was isolated from the lung tissue of the K and KM mice, respectively. PCR was performed with indicated primers, and the results showed successful deletion of the *Mkrn3* in the KM mice, but not in the K mice. **(E)** Areas of tumors in K and KM mice. Columns, percent of lung area occupied by tumors. K, *K-ras*$^{LSL-G12D/+}$ mice; KM, *K-ras*$^{LSL-G12D/+}$; *Mkrn3*$^{pfl/m+}$ mice. The data were summarized from 168 tumors in 10 K (K-ras$^{LSL-G12D/+}$) mice and 396 tumors in 14 KM mice.

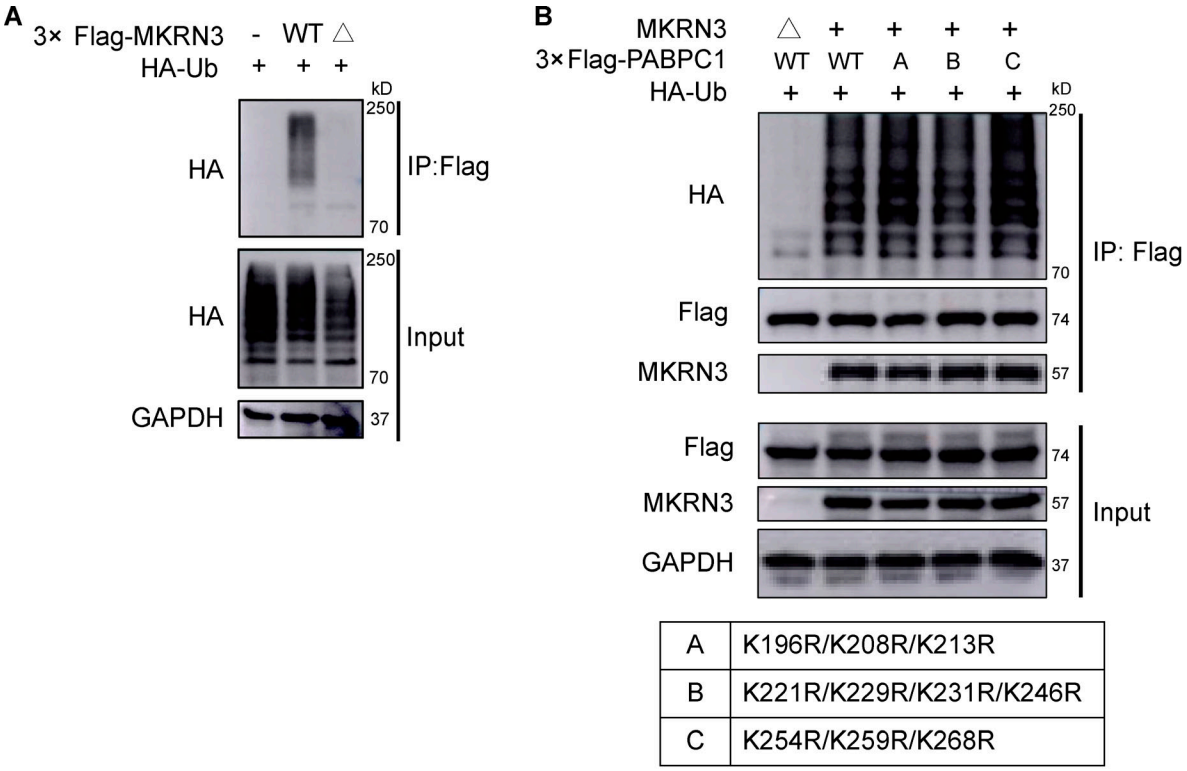

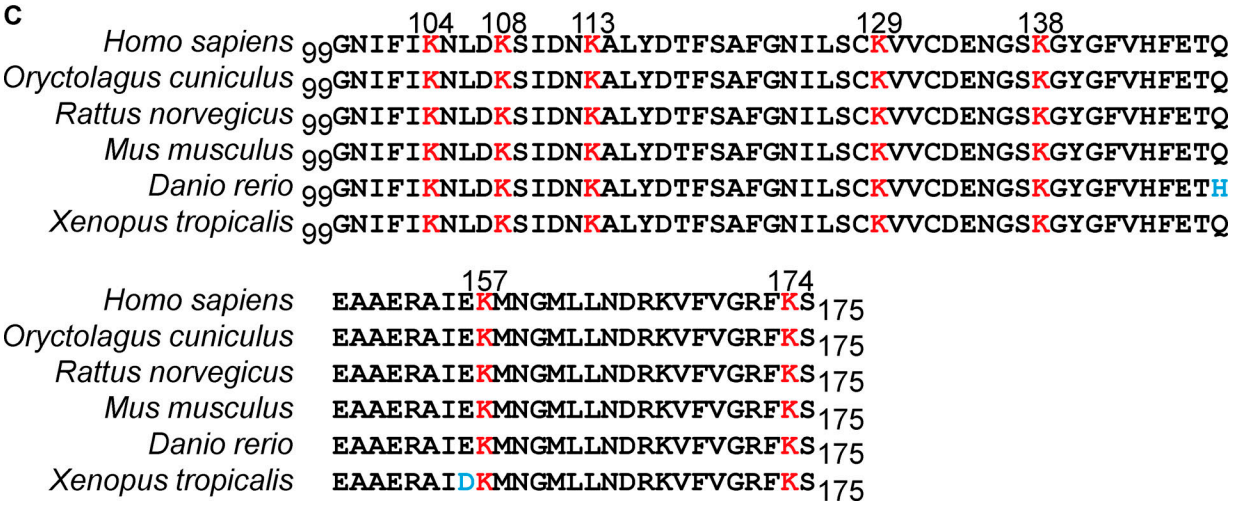

Figure S5. **MKRN3 mediates PABPC1 ubiquitination. (A)** *MKRN3* cancer-specific mutation compromise ubiquitination activity. Lung cancer–derived MKRN3 mutant (C258*, indicated by Δ) disrupts MKRN3-mediated ubiquitination. HEK293T cells were transfected with HA-Ub, WT MKRN3 (Flag-tagged), or C258* mutant MKRN3 (Flag-tagged) cDNA. Cell lysates were immunoprecipitated with anti-Flag antibody, followed by immunoblotting with anti-HA antibody. **(B)** The lysine residues in the RRM3 domain of PABPC1 are not subject to PABPC1 ubiquitination by MKRN3. HEK293T cells transfected with MKRN3, Flag-PABPC1 (WT or indicated K-to-R point mutants), and WT HA-Ub were immunoblotted for the indicated proteins on immunoprecipitated Flag-PABPC1. **(C)** PABPC1 Ub sites are conserved across different species. The seven lysine residues for the MKRN3-mediated ubiquitination of PABPC1 in RRM2 domain are conserved across human, rabbit, rat, mouse, zebrafish, and frog. All panels represent data from two independent experiments.

Tables S1, S2, S3, and S4 are provided as separate Excel files online. Table S1 shows clinicopathologic classification for 67 NSCLCs with genomic MKRN3 aberrations from TCGA lung cancer datasets. Table S2 shows clinicopathologic classification and MKRN3 protein expression in 30 NSCLCs from Asian patients. Table S3 shows gene expression profiling by RNA sequencing 96 hours after MKRN3 restoration in MKRN3-deficient/MKRN3-mutant H1703 cells. Table S4 shows primers used in the study.